The Nodule-Specific PLAT Domain Protein NPD1 Is Required for Nitrogen-Fixing Symbiosis[1][OPEN]

Catalina I. Pislariu,[a,b] Senjuti Sinharoy,[a,2] Ivone Torres-Jerez,[a] Jin Nakashima,[a] Elison B. Blancaflor,[a] and Michael K. Udvardi[a,3,4]

[a]Plant Biology Division, Noble Research Institute, Ardmore, Oklahoma 73401
[b]Department of Biology, Texas Woman's University, Denton, Texas 76204

ORCID IDs: 0000-0002-9647-5400 (C.I.P.); 000-0003-2323-2587 (S.S.); 0000-0001-6115-9670 (E.B.B.); 0000-0001-9850-0828 (M.K.U.).

Symbiotic nitrogen fixation by rhizobia in legume root nodules is a key source of nitrogen for sustainable agriculture. Genetic approaches have revealed important roles for only a few of the thousands of plant genes expressed during nodule development and symbiotic nitrogen fixation. Previously, we isolated >100 nodulation and nitrogen fixation mutants from a population of *Tnt1*-insertion mutants of *Medigaco truncatula*. Using *Tnt1* as a tag to identify genetic lesions in these mutants, we discovered that insertions in a *M. truncatula* nodule-specific polycystin-1, lipoxygenase, α-toxin (PLAT) domain-encoding gene, *MtNPD1*, resulted in development of ineffective nodules. Early stages of nodule development and colonization by the nitrogen-fixing bacterium *Sinorhizobium meliloti* appeared to be normal in the *npd1* mutant. However, *npd1* nodules ceased to grow after a few days, resulting in abnormally small, ineffective nodules. Rhizobia that colonized developing *npd1* nodules did not differentiate completely into nitrogen-fixing bacteroids and quickly degraded. *MtNPD1* expression was low in roots but increased significantly in developing nodules 4 d postinoculation, and expression accompanied invading rhizobia in the nodule infection zone and into the distal nitrogen fixation zone. A functional MtNPD1:GFP fusion protein localized in the space surrounding symbiosomes in infected cells. When ectopically expressed in tobacco (*Nicotiana tabacum*) leaves, MtNPD1 colocalized with vacuoles and the endoplasmic reticulum. *MtNPD1* belongs to a cluster of five nodule-specific single PLAT domain-encoding genes, with apparent nonredundant functions.

Crop and pasture legumes inject ~50 million tons of bioavailable nitrogen into agricultural systems annually by virtue of symbiotic associations with nitrogen-fixing bacteria of the family Rhizobiaceae (Graham and Vance, 2003). Symbiotic nitrogen fixation (SNF) in legumes involves the development of a specialized organ, the root nodule, which accommodates rhizobia and facilitates the exchange of nutrients between the host and intracellular microbes (Udvardi and Poole, 2013). As a prelude to symbiosis, legume roots release chemical signals (flavonoids) that induce the expression of nodulation genes in soil rhizobia that are required for the biosynthesis of lipochitooligosaccharide nodulation factors (NFs), which in turn act as signals to the plant, triggering biophysical, biochemical, and genetic responses that lead to nodule development and bacterial invasion of root and nodule cells (Geurts and Bisseling, 2002). The infection process involves attachment of rhizobia to root hair cells, root hair curling and "entrapment" of bacterial microcolonies, dissolution of the root hair cell wall, and invagination of the cell membrane to form a tube-like structure, the infection thread (IT), which enables rhizobia to enter the epidermal and underlying cells of the developing nodule primordium (Ardourel et al., 1994; Limpens et al., 2003). Rhizobia are eventually released from the IT into individual plant cells via endocytosis, which leaves them surrounded by a plant-derived membrane in cytoplasmic "organelles" called symbiosomes (Udvardi and Day, 1997; Brewin, 2004; Udvardi and Poole, 2013). Thousands of symbiosomes are accommodated in each infected host cell. Inside symbiosomes, rhizobia undergo endoreduplication and differentiation into nitrogen-fixing "bacteroids". *Medicago truncatula* nodules are generally cylindrical in shape and organized in distinct developmental and functional zones. Starting from the nodule apex, they include the meristematic

[1]This work was funded by the National Science Foundation Plant Genome Research Program (grants IOS-0703285 and IOS-1127155), the National Science Foundation Major Research Instrumentation (MRI) Program (grant DBI-0722635), and the Noble Research Institute.

[2]Present address: National Institute of Plant Genome Research, Aruna Asaf Ali Marg, P.O. Box No. 10531, New Delhi 110067, India

[3]Author for contact: mudvardi@noble.org

[4]Senior author.

The author responsible for distribution of materials integral to the findings presented in this article in accordance with the policy described in the Instructions for Authors (www.plantphysiol.org) is: Michael K. Udvardi (mudvardi@noble.org)

C.I.P and M.K.U. conceived the project and wrote the manuscript with contributions from all authors; C.I.P. designed the experiments, performed most of the work, and analyzed the data; S.S. and I.T-J. were involved in the experimental work and data analysis; S.S. complemented the writing; J.N. and E.B.B. provided technical assistance to C.I.P.

[OPEN]Articles can be viewed without a subscription.
www.plantphysiol.org/cgi/doi/10.1104/pp.18.01613

zone of active cell division; the infection zone, where rhizobia are released from ITs as symbiosomes; the distal nitrogen fixation zone, where bacteria undergo genome endoreduplication and elongation into functional bacteroids; the active nitrogen fixation zone; and, in older nodules, the senescence zone, where both bacteroids and their host cells degenerate (Vasse et al., 1990).

Nodule development and symbiotic metabolism are complex processes that involve the coordinated expression of thousands of plant and bacterial genes. Development of genetic and genomic resources for model legumes such as *M. truncatula* and *Lotus japonicus* has facilitated the discovery of some of the genes that are essential to these processes (Benedito et al., 2008; Sato et al., 2008; Tadege et al., 2008; Young et al., 2011; Couzigou et al., 2012; Fukai et al., 2012; Kryvoruchko et al., 2016; Sinharoy et al., 2016). Having elucidated much of the NF signaling pathway and many of the early steps preceding symbiosome release into host cells (Oldroyd et al., 2011), interest has shifted toward later aspects of symbiosis, including bacteroid differentiation, maintenance, senescence, and nitrogen fixation efficiency (Bourcy et al., 2013; Sinharoy et al., 2013; Berrabah et al., 2014a).

Accumulating evidence supports the idea that the host's immune system and microbial signals play critical roles in triggering either symbiotic or pathogenic responses (Berrabah et al., 2015). Transcriptomic studies revealed that defense mechanisms are induced during the initial stage of symbiosis, but various factors, including rhizobial exopolysaccharides and NFs, appear to repress host defense, ensuring successful infection and massive colonization (Jones et al., 2008; Rey et al., 2013; Cao et al., 2017). However, at later stages, defense mechanisms seem to be modulated rather than completely repressed. In *M. truncatula*, terminal differentiation of bacteroids involves inhibition of cell division and genome endoreduplication, which limits population growth, a process controlled by host defensin-like, nodule-specific Cys-rich peptides (NCRs; Mergaert et al., 2003, 2006). The bacterial differentiation A (BacA) protein is required to counteract the toxic effects of NCRs, and a *bacA* mutant does not survive in wild-type nodules (Haag et al., 2011). To gain access to bacteroids, NCRs are targeted to symbiosomes in a *Defective in Nitrogen Fixation* (*DNF1*)-mediated process (Wang et al., 2010). Terminal bacteroid differentiation and survival inside host cells has been shown to be controlled by at least four other host genes: *DNF2*, encoding a phosphatidylinositol phospholipase C-like protein (Bourcy et al., 2013); *Regulator of Symbiosome Differentiation* (*RSD*), encoding a C2H2 transcription factor (Sinharoy et al., 2013); *Symbiotic Cys-Rich receptor-like Kinase* (*SymCRK*), encoding a non-RD receptor-like kinase (Berrabah et al., 2014a); and *Nodules with Activated Defense 1* (*NAD1*), encoding a small peptide of unknown function (Wang et al., 2016).

Using a *Transposable element of tobacco* (*Nicotiana tabacum*) *cell type 1* (*Tnt1*)-insertion mutant population of *M. truncatula*, we previously isolated 179 symbiotic mutants (Pislariu et al., 2012). Only 39 of these were found to harbor *Tnt1* insertions in known symbiotic genes. In other words, many of these symbiotic mutants are likely to result from insertions in previously uncharacterized genes. With the aim of uncovering new genetic controls on bacteroid accommodation, we screened several *Tnt1*-insertion mutants with inefficient nodules for flanking sequence tags (FSTs) in nodule-specific genes. Here, we report the identification and characterization of a previously unknown symbiotic gene, *MtNPD1*, which encodes a protein with a single polycystin-1, lipoxygenase, α-toxin (PLAT) domain and is required for nodule development, accommodation of rhizobia inside host cells, and nitrogen fixation.

RESULTS

A Symbiotic Mutant Impaired in Nodule Development and Function

Starting with a collection of >100 symbiotic mutants of *M. truncatula* (Pislariu et al., 2012), we characterized in detail individuals of line NF4608, which exhibited a nitrogen-deficient phenotype with stunted shoots, chlorotic leaves that accumulated red pigment (probably anthocyanins), and small, white root nodules when grown under low nitrogen in the presence of *Sinorhizobium meliloti* Sm1021 (Fig. 1, A and B). At 21 d postinoculation (DPI), the average nodule number in NF4608 mutants was 65 ± 15, while wild-type plants developed 25 ± 7 nodules per plant (n = 25 plants; mean ± SD; Fig. 1C). The average nodule length of NF4608 mutants at 21 DPI (0.53 ± 0.2 mm) was significantly smaller than for the wild type (1.62 ± 0.3 mm, n = 25 plants, mean ± SD; Fig. 1D).

To determine whether the reduced nodule size of the mutants was caused by delayed nodule initiation, slower nodule development, or premature senescence, nodule sizes were compared at 6, 8, 10, 12, and 15 DPI for NF4608 mutant and wild-type (R108) plants. The onset of nodulation in NF4608 was synchronous with that of the wild type, but nodules stopped growing at 8–10 DPI and lacked the pink coloration due to leghemoglobin, characteristic of wild-type nodules (compare Supplemental Fig. S1, A–E and F–J). The symbiotic phenotype of the mutant was assessed further, using as inoculum *S. meliloti* strain Sm1021, which carries a *hemA*:*lacZ* reporter gene. The 5-bromo-4-chloro-3-indolyl-β-D-galactopyranoside (blue)-staining of *lacZ*-expressing rhizobia revealed that nodules of the mutant harbored fewer rhizobia than those of the wild type from 8 DPI onward (Fig. 1, E–J). Rhizobia were observed primarily in the distal zone of mutant nodules at 10 DPI, with virtually no rhizobia in the central zone of these nodules, in stark contrast to the wild type (compare Fig. 1, G and J). ITs in NF4608 mutants appeared normal in most cases, although occasional abnormalities were observed, such as irregular proliferation inside root hairs and in the root hair curl (compare Supplemental Fig. S1, K–M) or release of

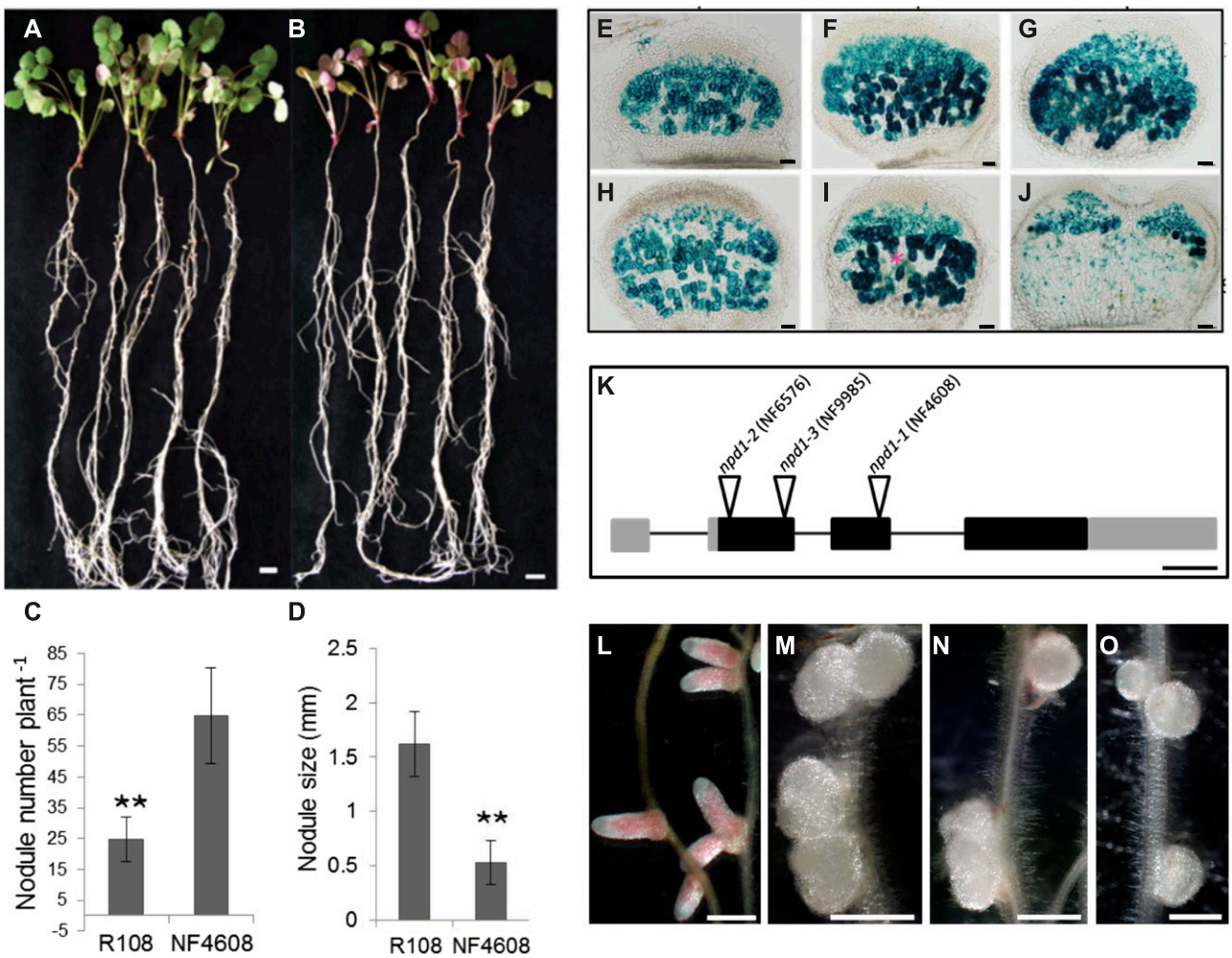

Figure 1. Symbiotic phenotype of the NF4608 mutant. A and B, Wild-type R108 (A) and NF4608 mutant (B) plants at 21 DPI with *S. meliloti* strain Sm1021. C and D, Average nodule number and size in wild-type R108 (C) versus NF4608 mutants (D). Vertical bars represent the SD from measurements in 20 R108 and 35 NF4608 mutants. Asterisks indicate a significant difference compared to the control, as determined using Student's *t* test ($P \leq 0.01$). E to J, Histochemical staining of *S. meliloti* Sm1021 carrying the *hemA:LacZ* reporter in wild-type (E–G) and NF4608 mutants (H–J). The rhizobia stain blue. Shown are 50-μm-thick slices from nodules at 6 DPI (E and H), 8 DPI (F and I), and 10 DPI (G and J). K, Schematic representation of the *MtNPD1* gene structure displaying exons in black, introns as a line, and the 5′ and 3′ untranslated regions in gray. *Tnt1* insertion sites in three independent alleles are shown. Symbiotic phenotypes of wild-type (L) and three *npd1* insertion alleles: *npd1-1* (M; NF4608); *npd1-2* (N; NF6576); *npd1-3* (O; NF9985) are shown. Scale bars = 1 cm (A and B), 50 μm (E–J), 100 bp (K), and 1 mm (L–O).

rhizobia inside epidermal cells (Supplemental Fig. S1N). At the nodule primordium stage (4 DPI), when ITs had reached dividing inner cortical cells and started to release rhizobia in the wild type (Supplemental Fig. S1O), some ITs appeared to be blocked in the outer cell layers of the cortex or in the epidermis of the mutant (Supplemental Fig. S1P).

A *Tnt1* Insertion in a Nodule-Specific PLAT Domain Gene, *MtNPD1*, Is Responsible for the Symbiotic Defect

Genomic DNA extracted from leaves of NF4608 mutants was subjected to thermal asymmetric interlaced PCR followed by Sanger sequencing to retrieve genomic regions adjacent to *Tnt1* insertion sites. Illumina sequencing was also carried out. One FST from NF4608 corresponded to a nodule-specific gene, *Medtr2g103303.1* (*M. truncatula* Gene Expression Atla; Benedito et al., 2008). Gene annotations of additional FSTs are shown in Supplemental Table S1.

A NF4608 symbiotic mutant was backcrossed with wild-type R108 (BC_1) and resulting F1 individuals were self-fertilized to generate F2 seed (BC_1 F2). A total of 85 BC_1 F2 plants were analyzed for symbiotic phenotypes and 61 displayed the wild-type, effective nitrogen fixation (Fix^+) phenotype, while 24 plants exhibited an ineffective (Fix^-) phenotype. This ratio (~3:1) indicated that the Fix^- phenotype resulted from a monogenic, recessive mutation ($\chi^2 = 0.476$; $P \leq 0.05$). Mutant BC_1

F2 plants were backcrossed a second time with wild-type R108, and segregation analysis of 70 plants in the BC_2 F2 population yielded 19 Fix^- plants and 51 Fix^+ plants, again consistent with an expected ratio of 3:1 ($\chi^2 = 0.311$; $P \leq 0.005$). Genotypic analysis using primers specific to *Medtr2g103303.1* (NPD1-ENTR-F and NPD1-ENTR-R1) and *Tnt1* (Supplemental Table S2) was carried out on BC_1 F2 Fix^+ and Fix^- plants. "ENTR" denotes that the NPD1 forward and reverse primers were used to clone the MtNPD1 coding sequence into the pENTR-D-TOPO vector. Homozygous *Tnt1* insertions in *Medtr2g103303.1* were always and only found in Fix^- individuals, indicating a causal relationship between the insertion in this gene and the phenotype. Cloning and sequencing of PCR products spanning the site of the *Tnt1* insertion in *Medtr2g103303.1* confirmed insertion in the second exon, 474 bp downstream of the ATG start codon (Fig. 1K).

MtNPD1 was cloned from complementary DNA synthesized from R108 functional nodules and was found to consist of three exons of 135 bp, 123 bp, and 243 bp, respectively (Fig. 1K). By aligning the cloned *MtNPD1* coding sequence from R108 (*MtNPD1*_R108) with the genomic region of *MtNPD1* in *M. truncatula* Jemalong A17 (Mt4.0v1; http://www.medicagogenome.org/) we found a few nucleotide mismatches and a 9-bp nucleotide deletion in MtNPD1_R108, shown in Supplemental Figure S2, green line. Despite the observed mismatches with the A17 reference genome (Mt4.0v1), the coding sequence of the cloned *MtNPD1* of R108 matched perfectly with the R108 genomic sequence (R108 v0.95 genome assembly; http://medicago.jcvi.org; Supplemental Fig. S3).

The putative protein encoded by *Medtr2g103303.1* contains a signal peptide (SP) region (amino acid residues 1–21), as determined with the SignalIP 4.1 tool (Kalandadze et al., 1990) and a PLAT (also known as lipoxygenase homology) domain (IPR001024; amino acid residues 54–163), according to the National Center for Biotechnology Information Conserved Domain Search Tool (Marchler-Bauer et al., 2015). In light of its nodule-specific expression pattern (Benedito et al., 2008; He et al., 2009), we named the gene *Nodule-Specific PLAT Domain 1*, *MtNPD1*.

Two additional *npd1* mutant alleles were identified by PCR screening of pooled DNA from the *Medicago Tnt1*-insertion mutant population, using nested gene-specific primers NPD1-F2, NPD1-F3, NPD1-R4, and NPD1-R6, and *Tnt1* primers *Tnt1* Fw (forward), *Tnt1* Fin (forward inner), *Tnt1* Rin (reverse inner), and *Tnt1* Rev (reverse; Supplemental Table S2). *Tnt1* was found in the first exon, 46 bp downstream of the ATG start codon in line NF6576, and, also in the first exon, 124 bp downstream of ATG in line NF9985 (Fig. 1K). Additional FSTs from NF6576 and NF9985 are available in the *Medicago* mutant database (http://medicago-mutant.noble.org), and their IMGAG v4.0 annotations are listed in Supplemental Table S1. Thus, three mutant alleles of *MtNPD1* were isolated: *npd1-1* (NF4608), *npd1-2* (NF6576), and *npd1-3* (NF9985). Descendants of all three mutant lines displayed identical defective symbiotic phenotypes: reduced plant growth with supernumerary, small, white nodules when inoculated with *S. meliloti* Sm1021 and grown under nitrogen-limited conditions (Fig. 1, L–O). Cosegregation analyses in BC_1 F2 populations of the *npd1-2* and *npd1-3* mutants confirmed linkage between disrupted *MtNPD1* and defective symbiosis.

In order to confirm that loss of NPD1 function caused the aberrant symbiotic phenotype of the *npd1-1* mutant, roots of the mutant were transformed with the wild-type *MtNPD1* gene driven by the constitutive Cauliflower mosaic virus 35S promoter (*p35S:MtNPD1*) and inoculated with rhizobia. Green-fluorescent transgenic *npd1-1* roots expressing both the *MtNPD1* and *GFP* genes produced fewer and larger nodules than transgenic roots of *npd1-1* expressing *GFP* but not *MtNPD1* (Fig. 2). Nodules on *npd1-1* roots expressing wild-type *MtNPD1* were pink, in contrast to the white nodules of the mutant (Fig. 2, C–F), and apparently effective, given the larger size and greenness of leaves of the *NPD1*-expressing plants (Fig. 2, A and B). Acetylene reduction assays revealed a 10-fold increase in nitrogen fixation capacity in *MtNPD1*-complemented *npd1-1* roots compared to *npd1-1* roots transformed with the vector control (Fig. 2G).

Although *npd1* plants grew poorly when reliant upon rhizobia as the primary source of nitrogen (Fig. 1), they grew well, like the wild type, when supplied with sufficient mineral nitrogen, as shown by plant appearance (Supplemental Fig. S4A) and whole plant biomass (Supplemental Fig. S4B).

SNF Is Impaired in All Three *npd1* Mutants

Nitrogenase activity of nodulated *npd1-1*, *npd1-2*, and *npd1-3* mutant plants was assayed by measuring acetylene reduction. Acetylene reduction (ethylene production) was virtually nil at 15 DPI in each of the mutants, in contrast to the wild type (Fig. 3A). To assess nitrogen fixation at earlier time points, transcript levels of the nitrogen fixation H (*nifH*) gene, which encodes a nitrogenase subunit (Ruvkun et al., 1982), were measured by quantitative PCR (qPCR), before inoculation and at 3, 6, and 10 DPI in the wild type and the *npd1-1* mutant. *nifH* expression was barely detectable in *npd1-1* at 10 DPI (Fig. 3B). Using an *S. meliloti* strain carrying a *nifH:GFP* reporter gene, we found that the *nifH* promoter was essentially silent in 15 DPI nodules of *npd1-1*, again in contrast to the wild type, in which GFP fluorescence was observed throughout the nitrogen fixation zone of nodules (Fig. 3, C–F). NifH is an essential component of the nitrogenase nifHDK enzyme complex, and lack of expression of any one of the corresponding genes could account for the absence of nitrogen fixation in the *npd1* mutants.

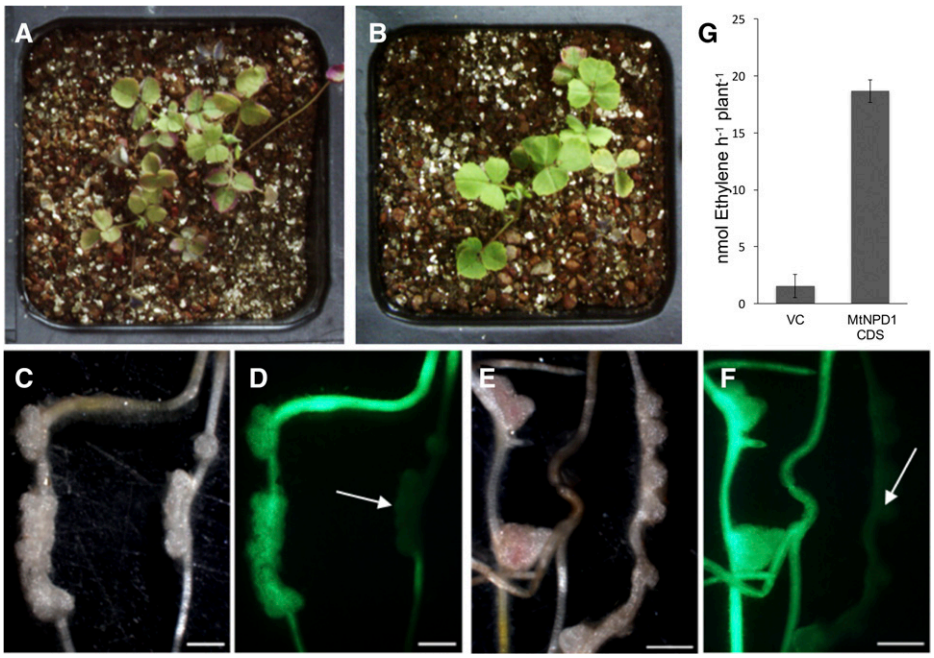

Figure 2. Genetic complementation of the *npd1-1* mutant by *p35S:MtNPD1*. *R. rhizogenes*-mediated transformation was used to rescue the wild-type phenotype in the *npd1-1* mutant by cloning the coding sequence of wild-type *MtNPD1* driven by the 35S promoter into *npd1-1* plants. A, C, and D, Images of *npd1-1* plants transformed with an empty vector control. B, E, and F, Images of *npd1-1* plants transformed with *p35S:MtNPD1*. Green fluorescence in D and F is given by the GFP marker in the complementation plasmid backbone and indicates transgenic roots. The white arrows point towards *npd1-1* roots that failed to transform with the vector control (D) and with the p35S:MtNPD1 construct (F). G, Acetylene reduction activity in whole nodulated roots from 10 composite plants transformed with the vector control (VC) and 11 *npd1-1* plants transformed with p35S:*MtNPD1*. Vertical bars represent the SE. Photomicrographs in C to F were acquired with an Olympus SZX12 fluorescence stereomicroscope. CDS = coding sequence. Scale bars = 1 mm.

MtNPD1 Is Required for Stable Accommodation and Differentiation of Rhizobia

To gain further insight into the symbiotic defect in *npd1* mutants, a thorough microscopic analysis of nodules was carried out. Semithin 1-μm sections of 12 DPI wild-type and *npd1-1* nodules were imaged after toluidine blue O staining (Fig. 4). Besides being smaller, *npd1-1* nodules did not display the successive developmental zones typical of young, functional, indeterminate nodules of *Medicago*: meristem, infection zone, distal nitrogen fixation zone, and nitrogen fixation zone (Fig. 4A). Instead, a wider infection zone was seen in *npd1-1* nodules, adjacent to which was a zone where rhizobia appeared to be degraded (Fig. 4E). Higher-magnification images of the infection zone showed that rhizobia were released from ITs in *npd1-1* plants but few plant cell layers were filled with symbiosomes, in contrast to wild-type nodules (compare Fig. 4, B and F). Furthermore, misshapen vacuoles and nuclei were observed in cells of the infection zone proximal to the root, and into the junction with the senescence-like zone in the *npd1-1* mutant. Rhizobia remained smaller and less elongated in the *npd1-1* mutant than in symbiosomes of the wild type (Fig. 4F). In contrast to the wild type (Fig. 4, C and D), *npd1-1* nodule cells of the infection zone proximal to the root had aberrant cellular organization with disintegrated symbiosomes, nuclei, and vacuoles (compare Fig. 4, C and D with Fig. 4, G and H).

Nodule sections were also viewed with a confocal microscope after staining DNA with the fluorescent dye Syto13 and cell walls with calcofluor white. In contrast to wild-type R108 nodules that were largely occupied by infected cells packed with green fluorescent Syto13-stained bacteria, *npd1-1* nodules harbored bacteria only within a narrow strip of cells in the infection zone (Supplemental Fig. S5, A and B). The bulk of *npd1-1* nodule tissue was occupied by cells virtually devoid of rhizobia. Furthermore, in contrast to the wild-type, green fluorescence from host cell nuclei was not visible in all *npd1-1* nodule cells (Supplemental Fig. S5, C and D).

Transmission electron microscopy was used to examine the ultrastructure of 12 DPI nodules of *npd1-1* and the wild type. Infected cells of the invasion zone contained newly released rhizobia, which appeared to have normal morphology in the *npd1-1* mutant (Fig. 5, A and B). Plant cell nuclei and nucleoli were clearly discernible in both wild-type and *npd1-1* plants. Although symbiosomes had comparable morphology in

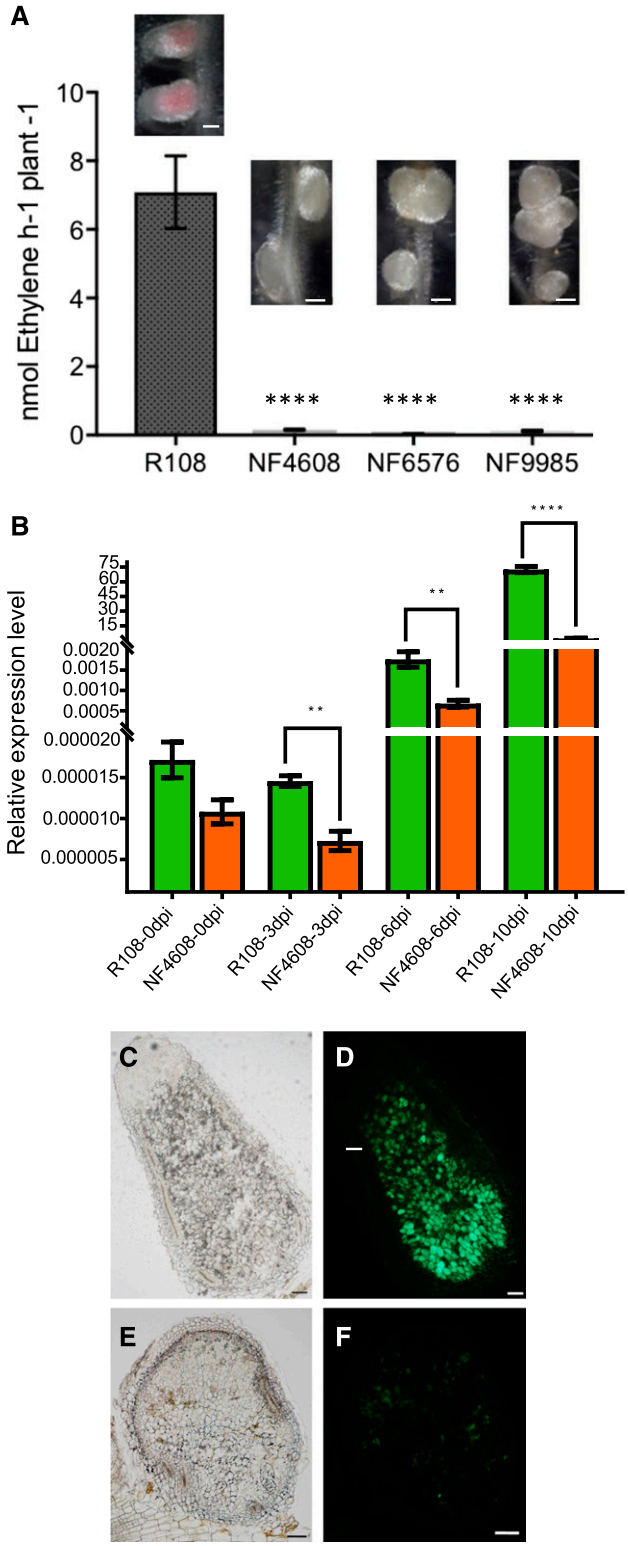

Figure 3. Rhizobia in three *npd1* mutants do not fix nitrogen. A, An acetylene reduction assay was carried out at 15 DPI on whole nodulated roots of the wild type (R108) and mutants of three independent *npd1* insertion alleles: *npd1-1* (NF4608), *npd1-2* (NF6576), and *npd1-3* (NF9985). Representative photos of nodule phenotypes are depicted above each bar. Data represent mean values measured in 37 R108 plants, 40 *npd1-1* plants, 45 *npd1-2* plants, and 49 *npd1-3* plants. Asterisks indicate significant differences between the wild type and mutants. $****P < 0.0001$. B, Rhizobial *nifH* gene expression was assessed by RT-qPCR during a nodule developmental time course (0, 3, 6, and 10 DPI). Green bars indicate relative expression of transcripts in the wild type, and orange bars indicate relative gene expression in the *npd1-1* mutant. Asterisks indicate a significant difference between R108 and *npd1-1*. $**P < 0.01$. In A and B, vertical bars indicate the SE and significant difference is based on one-way ANOVA tests with correction for multiple comparisons. Bar graphs and statistical analyses were carried out using Prism 7 (GraphPad). C to F, Images of wild-type (C and D) and *npd1-1* mutant nodules (E and F) inoculated with Sm1022 carrying the *nifHp:GFP* reporter. Bright-field images (C and E) are juxtaposed against images with *NifH* gene expression visualized as GFP fluorescence (D and F). Images were acquired using an Olympus BX41 microscope equipped with an Olympus DP72 camera, using bright-field and GFP channel settings. Scale bars = 1 mm (A) and 100 μm (C–F).

the mutant and wild type, some exhibited expansion of the symbiosome space (Fig. 5B, black arrowheads). Within two to three cell layers proximal to the invasion zone, bacteria in *npd1-1* plants were elongated, but not to the degree typical of terminally differentiated bacteroids (compare Fig. 5, C and D). Some *npd1-1* symbiosomes accumulated dark, electron-dense material, while plant cell nuclei exhibited unusual texture (Fig. 5D). Cellular debris and symbiosomes lacking bacteroid content were observed in cells of the senescence-like zone (Fig. 5D, bottom). Bacteria/symbiosomes exhibited a radial distribution in cells of the wild type but not those of *npd1-1* nodules (Fig. 5, C and D).

A dual staining method was used to probe the viability of rhizobia in nodules at 8 and 10 DPI, as previously described (Haag et al., 2011). Freshly harvested wild-type (R108) and *npd1-1* nodules were sliced into 100-μm sections and immediately stained with a mixture of two fluorescent nucleic acid dyes: Syto9 (a membrane-permeable green-emitting dye) and propidium iodide (PI; a membrane-impermeable red-emitting dye). Nodule sections were imaged by confocal microscopy. At 8 DPI, bacteroids in both wild-type and *npd1-1* nodules stained green, indicating uptake of Syto9 but not PI (Supplemental Fig. S6, A, B, E, and F). However, at 10 DPI, only two to three cell layers of the invasion zone contained green rhizobia in *npd1-1* nodules, while bacteria throughout wild-type nodules stained green (Supplemental Fig. S6, C, D, G, and H). Proximal to the band of two to three cells with green-stained rhizobia in *npd1-1* nodules were two to three cell layers in which rhizobia stained red, indicating PI-permeable symbiosome and bacterial membranes (Supplemental Fig. S6, G and H). Infected cells closer to the central part of *npd1-1* nodules failed to stain with either Syto9 or PI, presumably because bacteria had disintegrated at this point (Fig. 5D; Supplemental Fig. S6 H). Interestingly, some bacteria within ITs of *npd1-1* also stained with PI, indicating that the structural integrity of the IT and/or bacterial membranes were

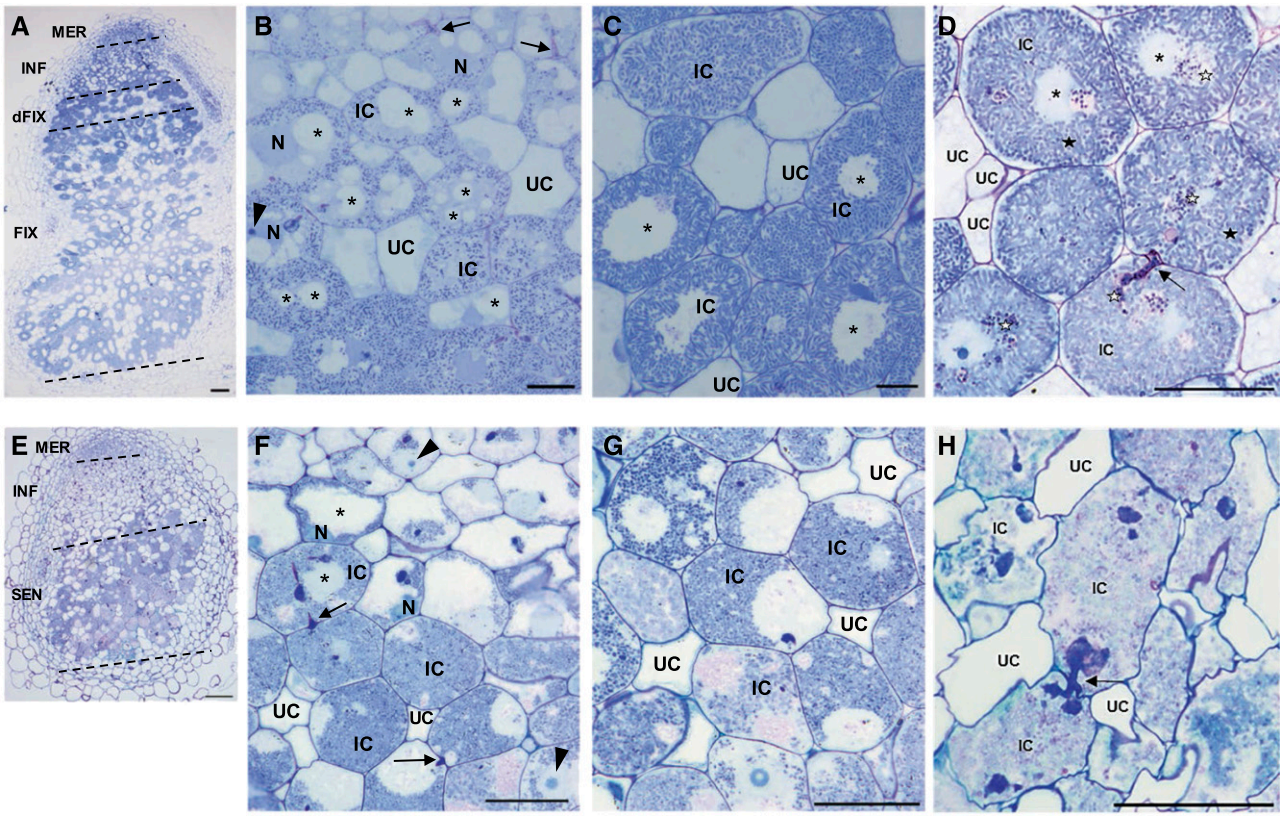

Figure 4. *MtNPD1* is required for the accommodation of rhizobia inside host cells. Longitudinal, 1 μm-thick sections of 12 DPI R108 (A to D) and *npd1-1* (E to H) nodules were stained with toluidine blue O. A and E, images show the different zones in wild-type (A) and mutant (E) nodules. Other images correspond to cells in the proximal infection zone (B and F; INF) and the distal nitrogen fixation zone (C; dFIX) in the wild type, infected cells in the junction area between the infection zone (INF) and the senescence zone (SEN) in the *npd1-1* mutant (G), infected cells in the nitrogen fixation zone (FIX) in the wild type (D), and infected cells in the senescence-like zone (SEN) in the *npd1-1* mutant (H). N, nuclei; IC, infected cell; UC, uninfected cell; MER, meristem.. Asterisks, vacuoles; arrowheads, nucleoli; arrows, ITs; ☆, newly released rhizobia; ★, differentiated rhizobia. Scale bars = 100 μm.

compromised even at this early stage of the symbiosis (Supplemental Fig. S6 H).

Taken together, microscopic examination of nodules of the *npd1* mutants and wild-type R108 indicated that *MtNPD1* is required to maintain viable rhizobia bacteria within host cells.

The Symbiotic Phenotype of *npd1* Mutants Is Strain Dependent

While conducting nodulation assays on *npd1-1 and npd1-2* mutants using *S. meliloti* strains Sm2011 or Sm1021 as inocula, we noticed striking differences in the appearance of mutant nodules. When inoculated with Sm1021, *npd1-1* nodules were small and white (Figs. 1–3 and 6A; Supplemental Figs. S1 and S4A). However, when inoculated with Sm2011, mutant nodules were small and accumulated dark brown material (Fig. 6B). Histochemical staining of 1-μm sections of wild-type R108 and *npd-1-1* nodules with potassium permanganate showed that the brown material in Sm2011-containing *npd1-1* nodules was probably phenolic in nature (Supplemental Fig. S7, C and D). To further explore the strain-dependent phenotype, homozygous *npd1-1* plants were inoculated with two additional strains, SmABS7 and Rm41. When inoculated with SmABS7, *npd1-1* plants developed mostly small, brown nodules, although a few large, pink nodules also developed (Fig. 6C). In contrast to all other strains, Rm41 rhizobia induced the development of large, pink nodules on *npd1* mutants (Fig. 6D). The total number of nodules and the number of pink nodules that developed on *npd1-1* mutants after inoculation with Rm41 rhizobia were higher than on wild-type plants, as was the associated shoot biomass (Fig. 6, E and F).

MtNPD1 Belongs to a Cluster of Five Nodule-Specific PLAT Domain-Encoding Genes

A BLAST search of the *M. truncatula* A17 genome, using the *MtNPD1* genomic sequence (http://medicago.jcvi.org)

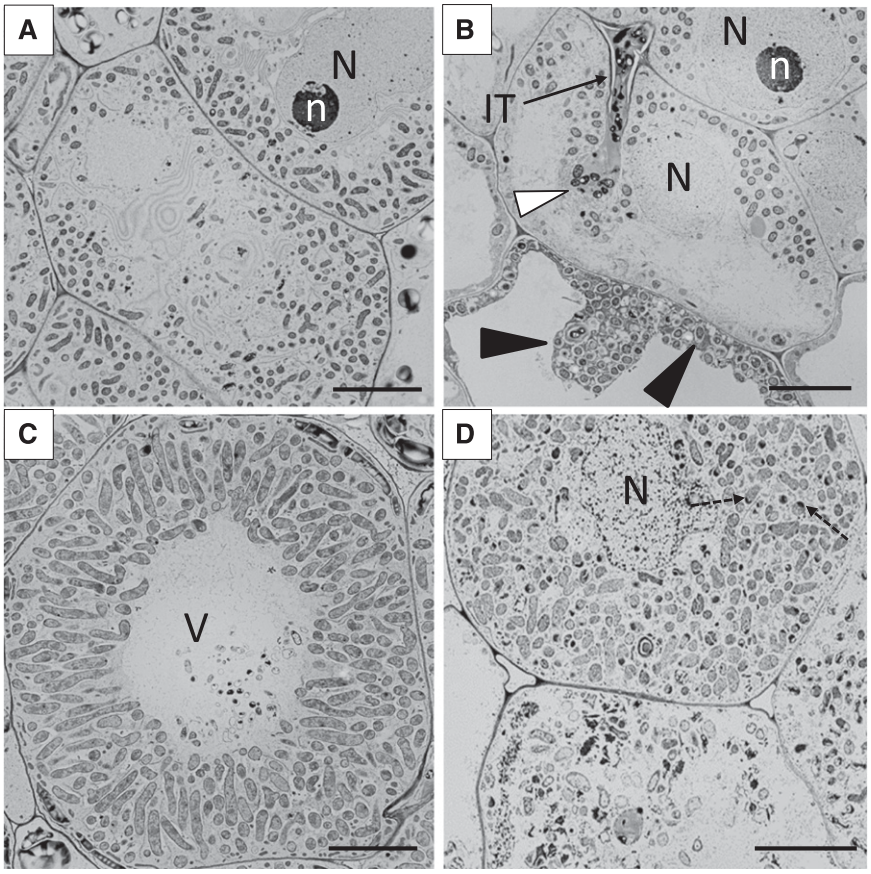

Figure 5. Bacteroids in *npd1* mutants disintegrate before they fully differentiate. Transmission electron microscopy images were acquired from 12 DPI wild-type (A and C) and *npd1-1* nodules (B and D). Photomicrographs represent the infection zone (A and B), the distal nitrogen fixation zone in the wild type (C), and the junction between the proximal infection zone and the senescence zone in the *npd1-1* mutant (D). White arrowhead, rhizobia being released; black arrowheads, symbiosomes with enlarged symbiosome space; dotted arrows, electron-dense material in symbiosomes; solid arrow, IT; N, nucleus; n, nucleolus; V, central vacuole. Scale bars = 10 μm.

yielded 13 homologous genes (Supplemental Table S3). Nine of these are annotated as "embryo-specific protein", and four others are annotated as "PLAT-plant-stress protein" (Mt4.0v1; Young et al., 2011; Tang et al., 2014). The *Medicago* Gene Expression Atlas was used to determine the expression patterns of these genes in various plant organs and treatments (http://mtgea.noble.org/v3/). Five of these genes were found to be nodule specific: *Medtr2g103303* (*MtNPD1*, described in this work), *Medtr2g103307*, *Medtr2g103313*, *Medtr2g103330*, and *Medtr2g103360*, corresponding to Affymetrix probe sets Mtr.49594.1.S1_at (*MtNPD1*), Mtr.20161.1.S1_at, Mtr.49593.1.S1_at, Mtr.49590.1.S1_at, and Mtr.49589.1.S1_at, respectively (Supplemental Fig. S8). In light of their nodule-specific expression, we propose renaming these as *Nodule-Specific PLAT Domain* genes (*MtNPD1* to *MtNPD5*). Notably, all five genes are located on chromosome 2, within a 30-kb region (Supplemental Fig. S9).

Proteins containing a PLAT domain and lacking other functional domains are common in plants (Supplemental Table S4). Forty representative proteins from plants (highlighted in Supplemental Table S4), including all 13 *Medicago* proteins, were used to generate an unrooted maximum-likelihood phylogenetic tree, using phylogeny based on maximum likelihood and the Le and Gascuel substitution model (Geneious 10.2.5; Fig. 7; Le and Gascuel, 2008). MtNPD1 groups together with all nodule-specific *Medicago* PLAT proteins and with an uncharacterized *L. japonicus* protein (Lj_I3SN54) that is expressed in nodules and flowers (Probeset chr3.TM0916.11.2_at in the *Lotus japonicus* Gene Expression Atlas, https://ljgea.noble.org). The *Medicago* PLAT-plant-stress proteins (MtPLAT5, MtPLAT6, MtPLAT7, and MtPLAT8) belong to a subgroup that includes the Arabidopsis (*Arabidopsis thaliana*) PLAT-domain proteins AtPLAT1, AtPLAT2, and AtPLAT3 (Hyun et al., 2014). Other known PLAT-domain proteins included in the tree are the *Capsicum annuum* tobacco mosaic virus-induced clone 1 (Shin et al., 2004) and *C. annuum* pathogen-induced protein 2 (Lee et al., 2006).

Induction of *MtNPD1* Expression Accompanies Early Infection Events

According to the *Medicago* Gene Expression Atlas (MtGEAv3), *MtNPD1* is expressed exclusively in nodules. *MtNPD1* transcript levels were 1,000-fold higher in 4 DPI nodulated roots than in roots at 0 DPI, and nearly 1,500-fold higher in 10 DPI nodules than in 0 DPI roots (Benedito et al., 2008; He et al., 2009).

To extend the MtGEA data, reverse transcription qPCR (RT-qPCR) analysis was conducted on RNA isolated from symbiosis-competent root segments (for

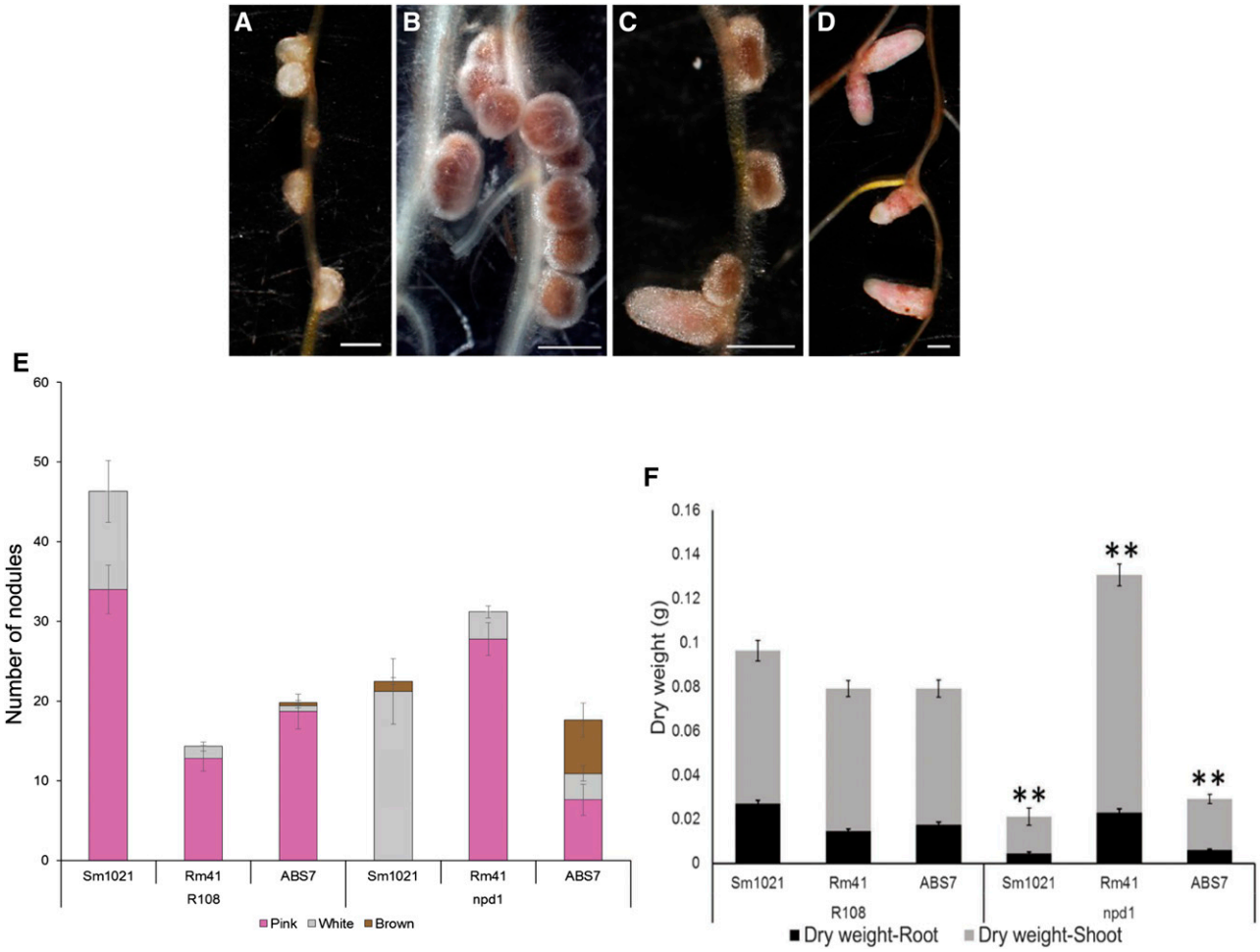

Figure 6. The symbiotic phenotype is strain dependent in the *npd1-1* mutant. A to D, Wild-type (R108) and *npd1-1* plants were inoculated with Sm1021 (A), Sm2011 (B), SmABS7 (C), and Rm41 (D). Phenotyping was carried out on plants at 6 weeks postinoculation. E, The number of pink, white, and brown nodules in R108 and *npd1-1* plants inoculated with Sm1021, Rm41, and SmABS7 is shown. F, Root and shoot biomass are calculated as the dry weight mean value from 15 samples for each combination of genotypes. Two biological replicates were carried out. For E and F, vertical bars represent the SE. Asterisks indicate a significant difference between *npd1-1* and R108 shoot biomass, as determined using Student's *t* test. $^{**}P \leq 0.01$. Scale bars = 1 mm.

early time points) and nodules (for later time points) of wild-type R108. *MtNPD1* transcripts increased significantly by 6 DPI (5,250-fold higher than in uninoculated roots) and reached a peak at 8 DPI (8,370-fold higher than in uninoculated roots; Fig. 8A). To gain spatial resolution, mature, 28 DPI wild-type A17 nodules were hand-sectioned into five developmental zones: the meristem, the infection zone, the distal nitrogen fixation zone, the nitrogen fixation zone, and the senescence zone, and *MtNPD1* transcripts were measured by RT-qPCR. *MtNPD1* transcript levels were highest in the nodule apex (meristem and infection zone; Fig. 8B).

In order to visualize *MtNPD1* expression in situ, an *MtNPD1* promoter-GUS (*pMtNPD1:GUS*) fusion construct containing 1,321 bp of sequence upstream of the start codon was transformed into *Medicago* R108 roots *via Rhizobium rhizogenes*. Composite plants were inoculated with Sm1021 expressing the *hemA:lacZ* reporter. In unfixed mature nodules (15 DPI), brief staining for β-galactosidase showed that *MtNPD1* expression was highest at the nodule apex and extended into the distal nitrogen-fixation zone (Supplemental Fig. S10). *MtNPD1* promoter activity was evident as early as 4 DPI in nodule bumps, including in epidermal cells containing ITs (Fig. 8, C and D). At 7 DPI, most activity was found in the nodule bump meristem and infection zone, as well as in patches of the outer cortex proximal to ITs (Fig. 8E). Because at 7 DPI accumulation of *MtNPD1* transcripts may have been masked by the magenta-Gal staining of rhizobia, to facilitate visualization of *MtNPD1* expression at 10 DPI, only GUS staining was carried out. At 10 DPI, GUS activity was observed in the infection zone and also in infected cells (Fig. 8F). Taken together, these results indicated that *MtNPD1* expression was active during the infection process and in infected cells.

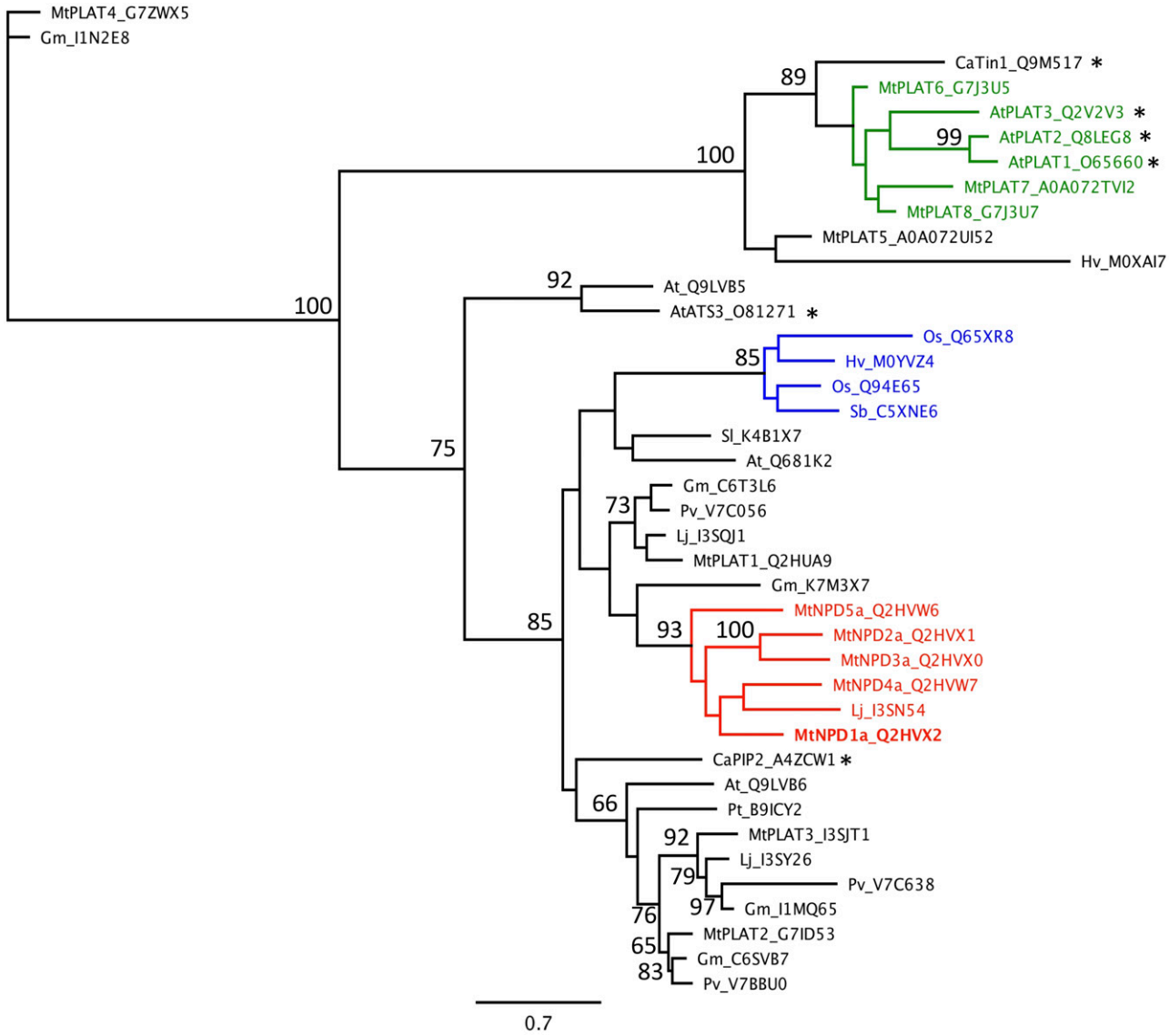

Figure 7. MtNPD1 belongs to a nodulation-specific clade of PLAT single-domain proteins. Full-length amino acid sequences of 40 plant PLAT domain proteins were aligned with ClustalW, and an unrooted maximum-likelihood phylogenetic tree was generated using PhyML and the LG substitution model (Geneious 10.2.5; Le and Gascuel, 2008). Numbers at branch nodes represent confidence values from 1,000 bootstrap replicates and indicate tree robustness. The scale bar represents the number of substitutions per site. The tree includes all members of the *Medicago* PLAT domain proteins found in the updated genome (Mt4.0v1; http://jcvi.org/medicago/). Proteins that have not previously been characterized are labeled with the two-letter species designation followed by the UniProt identifier. The nodule-specific clade is highlighted in red; the clade of proteins involved in biotic and abiotic stress response is highlighted in green, and the monocot clade is highlighted in blue. Bold fonts highlight MtNPD1. Asterisks mark proteins that have previously been described.

Dependence of *MtNPD1* Expression on Plant and Bacterial Symbiotic Genes

MtNPD1 expression was measured in nodules of various *Medicago defective in nitrogen fixation* mutants (*dnf1* to *dnf7*; Mitra and Long, 2004; Starker et al., 2006; Pislariu and Dickstein, 2007; Wang et al., 2010), and in the *Interacting Protein of DMI3* (*ipd3*; TE7) nodules, in which rhizobia are rarely released from deformed, hypertrophic ITs (Benaben et al., 1995; Horváth et al., 2011). *MtNPD1* was expressed in nodules of all *dnf* mutants, albeit at lower levels than in wild-type R108 nodules at 10 DPI (Fig. 9A). In contrast, *MtNPD1* was not expressed in *ipd3* (TE7) nodules at 10 DPI.

MtNPD1 gene expression was also measured in wild-type nodules elicited by three rhizobial mutants of strain 1021: an exopolysaccharide (*exoA*) mutant that is defective in the synthesis of exopolysaccharide EPS I and fails to be released from ITs inside nodule primordia (Leigh et al., 1985; Mitra and Long, 2004); a *bacA*

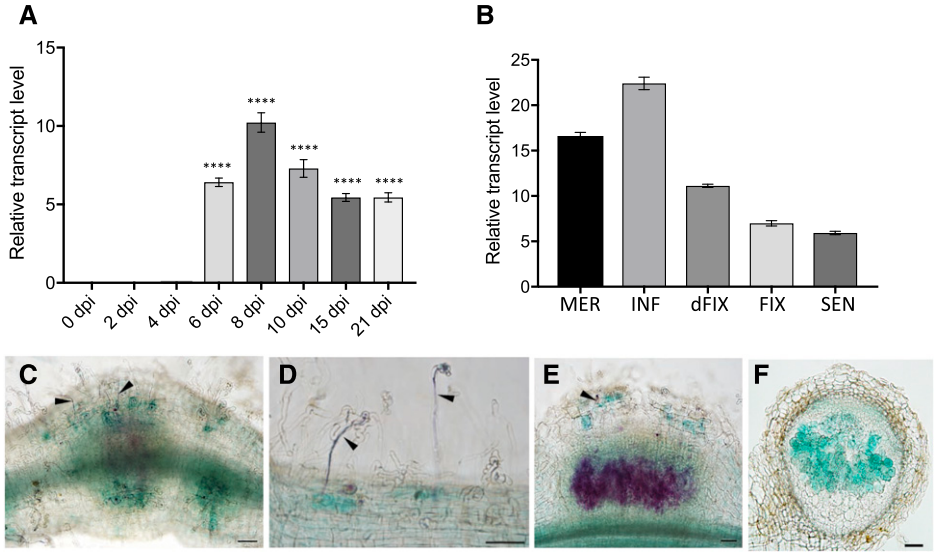

Figure 8. Spatiotemporal expression of *MtNPD1*. A, *MtNPD1* expression during a nodule development time course was measured by RT-qPCR. Nodulation-susceptible zones were used at 0 DPI and at 2 and 4 DPI (after inoculation with Sm1021). Samples at 6 to 21 DPI represent nodules dissected out of the roots. B, *MtNPD1* expression was also measured by RT-qPCR in the following hand-dissected nodule zones: the meristem (MER), the infection zone (INF), the distal nitrogen fixation zone (dFIX), the nitrogen fixation zone (FIX), and the senescence zone (SEN). RT-qPCR measurements were carried out on three biological replicates. C to F, p*MtNPD1:GUS* expression was observed in composite *M. truncatula* roots and nodules at 4 DPI (C and D), 7 DPI (E), and 10 DPI (F). Arrowheads point toward ITs. GUS coloration for promoter activity is blue. *S. meliloti* Sm1021 carrying the *hemA:LacZ* reporter was used for inoculation. Bacteria are seen as magenta precipitate in C to E, following histochemical staining for β-galactosidase activity. In F, only GUS coloration is shown. GUS and LacZ staining were carried out on whole roots. Images in C to E represent whole root mounts and that in F is a 50-μm-thick section. Scale bars = 100 μm. Error bars in A and B represent the mean ± SE. ****$P < 0.0001$, one-way ANOVA test followed by the Tukey posttest for multiple comparisons. Comparison is with 0 DPI.

mutant that is defective in differentiation into nitrogen-fixing bacteroids (Glazebrook et al., 1993; Oke and Long, 1999); and *fixJ*, which is a response regulator mutant that is released in infected cells and differentiates into nitrogen-fixing bacteroids, but undergoes early senescence (David et al., 1988; Oke and Long, 1999). *MtNPD1* was not expressed in nodules containing the *exoA* mutant at 10 DPI, but it was expressed in nodules containing *bacA* and *fixJ* mutants at levels slightly lower (*fixJ*) or considerably lower (*bacA*) than in nodules containing wild-type rhizobia (Fig. 9B).

In addition to *nifH* expression (see Fig. 3B), relative transcript levels of two more bacterial genes were measured during a nodulation time course in wild-type and *npd1-1* plants: *nifA*, which encodes a regulator of nitrogenase gene expression (Beynon et al., 1988), and *bacA*, which is required for bacterial survival inside infected cells (Haag et al., 2011). Similar to *nifH* (Fig. 3B), transcripts of *nifA* were extremely low in 10 DPI *npd1-1* nodules, while *bacA* transcript levels were similar in 10 DPI *npd1-1* mutant and wild-type nodules (Supplemental Fig. S11).

Intracellular Localization of MtNPD1

The coding sequence of MtNPD1 was fused to that of GFP and expressed in transformed root nodules of *Medicago* under the control of the *MtNPD1* promoter (*pMtNPD1:MtNPD1:GFP*). Free GFP driven by the *MtNPD1* promoter was used as a control and was found to accumulate in the nodule apex and in infected cells, consistent with the pattern of GUS activity resulting from *pMtNPD1:GUS* expression in transgenic nodules (Fig. 10, A and B; Supplemental Fig. S10). We found that the *pMtNPD1:MtNPD1:GFP* construct complemented the symbiotic defect of the *npd1-1* mutant, increasing acetylene reduction activity and ameliorating N-deficiency symptoms (Supplemental Fig. S12, A–C). In *MtNPD1:GFP*-complemented *npd1* nodules, green fluorescence was detected predominantly in the nodule infection zone, where rhizobia are released into host cells, and in infected cells of the distal nitrogen fixation zone (Fig. 10 C). In infected cells, MtNPD1:GFP fluorescence was observed in close proximity to symbiosomes (Fig. 9, D–F). Red fluorescent signal from Sm1021-mCherry rhizobia did not seem to overlap with the MtNPD1:GFP signal.

To gain further insight into the subcellular localization of MtNPD1, a red fluorescent protein (RFP) fusion construct driven by the 35S promoter was coexpressed with organelle markers in tobacco leaves (Supplemental Fig. S13, A–D). MtNPD1:RFP was observed as puncta of various sizes, which, for the most part, overlapped with the endoplasmic reticulum (Supplemental Fig. S13 B).

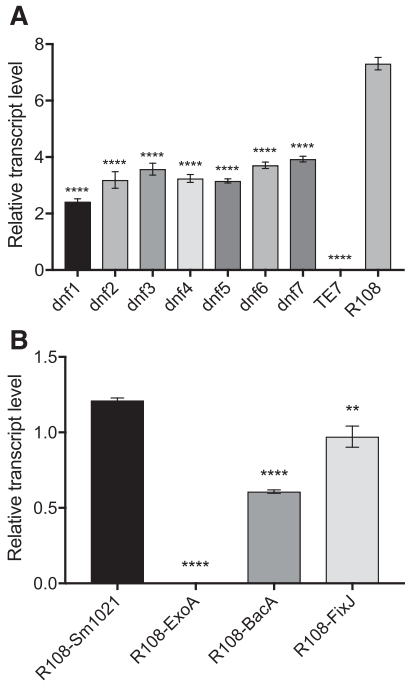

Figure 9. Relative expression of *MtNPD1* in Fix$^-$ nodules. Measurement of the relative *MtNPD1* transcript level was done in 10 DPI Fix$^-$ nodules from mutant plants with defects in plant genes (A) and bacterial genes (B). Column heights correspond to mean values from three independent biological replicates. Asterisks indicate comparison with wild-type (R108) nodules. Error bars show the SE. **$P < 0.005$; ****$P < 0.0001$; one-way ANOVA test with correction for multiple comparisons.

Some MtNPD1 puncta colocalized with vacuoles, suggesting that vacuolar-like compartments may be the final destination of MtNPD1 (Supplemental Fig. S13 A). No colocalization was observed with Golgi stacks, suggesting that MtNPD1 might belong to a Golgi-independent secretory pathway (Supplemental Fig. S13 C).

DISCUSSION

The *npd1* mutant described here is a novel symbiotic mutant characterized by arrested nodule development at an intermediate stage, altered nodule zonation, activated defense responses, and an inability of rhizobia to differentiate fully and fix nitrogen. After being released from ITs, rhizobia in developing *npd1* nodules elongated somewhat, but failed to differentiate into functional, nitrogen-fixing bacteroids, as demonstrated by cytological analyses and impaired acetylene reduction (Figs. 1, 3, 4, and 5). Furthermore, rhizobia were degraded sooner in *npd1* than in wild-type nodules (Figs. 4 and 5; Supplemental Figs. S5 and S6). In the infection zone, adjacent to the layer of cells containing newly released symbiosomes, plant cells harbored symbiosomes with enlarged symbiosome spaces around bacteria (Fig. 5B), suggesting that senescence can be induced very early during the infection process in *npd1* mutants. In Figure 5D, a more mature, fully infected cell harboring fairly normal symbiosomes is seen adjacent to a cell with signs of apoptosis (chromatin condensation, nuclear shrinkage, and fragmentation debris), in which distorted bacteroids contain electron-dense material. These findings suggest that senescence can be induced at different developmental stages in the *npd1* mutant. Symbiosome remnants were observed as empty structures with a visible peribacteroid membrane (PBM; Fig.. 5D, bottom; Supplemental Fig. S14). The nature of the electron-dense granules observed in these cells is not known, but similar structures have been observed in ineffective wild-type nodules containing *nif* mutant strains of *R. meliloti* (Hirsch et al., 1983).

An accumulation of brown pigment, illustrating plant defense responses and premature nodule senescence, has been reported in several SNF mutants, including *numerous infections and polyphenolics/lateral root-organ defective* (*nip/latd*), *does not fix nitrogen* (*dnf2*), *symbiotic cysteine-rich receptor-like kinase* (*symcrk*), *regulator of symbiosome differentiation* (*rsd*), and *nodules with activated defense 1* (*nad1*) mutants (Veereshlingam et al., 2004; Bourcy et al., 2013; Sinharoy et al., 2013; Berrabah et al., 2014a; Wang et al., 2016). Based on the observed phenotypes, we can group *npd1* mutants most closely with *rsd* and *nad1* mutants (Sinharoy et al., 2013; Wang et al., 2016). These three mutants exhibited underdeveloped, round nodules devoid of distal nitrogen-fixation and nitrogen-fixation zones, with signs of early senescence. In contrast, *dnf2* and *symcrk* nodules elongated nearly as much as those of the wild type and contained a nitrogen-fixation zone, which was narrower in *dnf2* than in *symcrk* (Berrabah et al., 2014a, 2014b). Both *dnf2* and *symcrk* mutants displayed early nodule senescence, although the onset of senescence occurred later than in *npd1*, *rsd*, and *nad1* mutants. All of these mutants accumulated brown material, indicative of defense responses. The expression profiles of these five genes during nodule development are similar, although relative expression levels vary, with transcript levels high for *MtNPD1* and low for *NAD1* (Supplemental Fig. S15; Benedito et al., 2008). It is possible that *MtNPD1*, *DNF2*, *RSD*, *NAD1*, and/or *SymCRK* are involved in the suppression of plant defense, although their involvement in stabilizing symbiosis may be indirect.

Differentiation of rhizobia into nitrogen-fixing bacteroids in *Medicago* is controlled by hundreds of nodule-specific Cys-rich peptides (NCRs) that are delivered through the endoplasmic reticulum secretory pathway (Van de Velde et al., 2010; Wang et al., 2010). A common fate of incompletely differentiated rhizobia is degradation. Recently, two NCRs required for bacterial survival in nodules have been identified: *DNF4* (*NCR211*; Kim et al., 2015) and *DNF7* (*NCR169*; Horváth et al., 2015). Although *dnf4* and *dnf7* mutant nodules remain small, they differ from those of *npd1* in a number of respects: they do not accumulate brown compounds; they proceed further in development and bacteroid

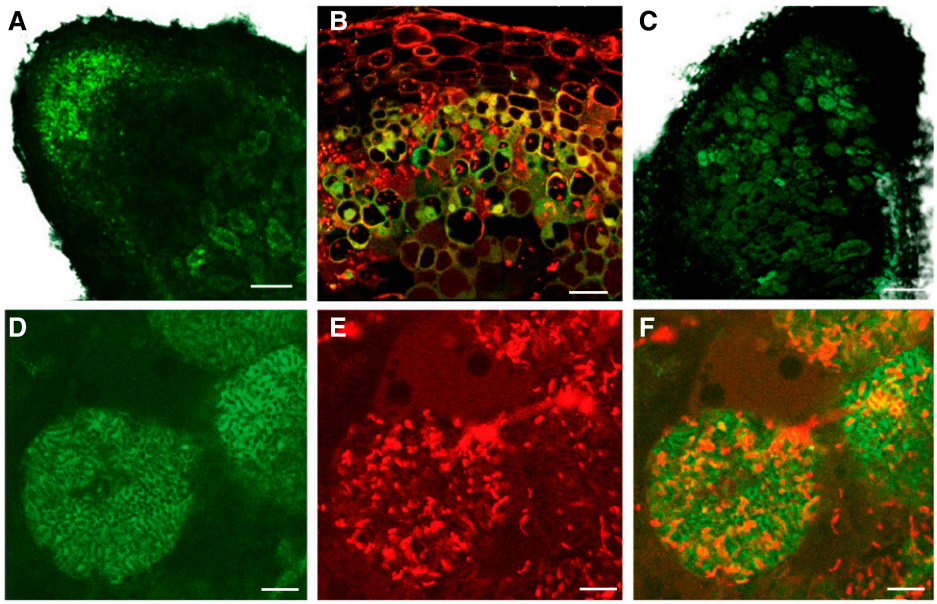

Figure 10. MtNPD1:GFP fusion driven by the native promoter localizes to the space surrounding symbiosomes in nodule infected cells. Transgenic nodules were harvested at 15 DPI, hand-sliced longitudinally, and immediately observed using a confocal laser scanning microscope. Images were acquired by sequential scanning using green and red fluorescence channels. A and B, GFP fluorescence driven by the *MtNPD1* promoter in R108 transgenic roots, used as a control. Accumulation of *MtNPD1* transcripts can be seen in the infection zone and in infected cells. The close-up image (B) shows a high level of *MtNPD1* promoter activity in the infection zone. C to F, Fluorescence of GFP fused to the C terminus of MtNPD1, driven by the native promoter, in complemented nodules of the *npd1-1* mutant. A and C represent overlays of GFP and transmitted light images. Red fluorescence in B, E, and F is from Sm1021 rhizobia carrying the mCherry reporter plasmid. (C and D) MtNPD1p:MtNPD1:GFP; (E) mCherry rhizobia; (F) Merge of D and E. Scale bars = 100 μm (A and C), 20 μm (C), and 10 μm (D to F).

differentiation; and they have normal nodule zonation, although the longevity of functional bacteroids in the nitrogen fixation zone is compromised (Horváth et al., 2015; Kim et al., 2015).

Developmental senescence in nodules and the associated degradation of bacteroids typically occur between 5 and 11 weeks after nodule inception. Brown pigmentation is usually not observed in senescing wild-type nodules (Van de Velde et al., 2006). Instead, the senescence zone is greenish, due to bilirubin accumulation resulting from leghemoglobin breakdown (Lehtovaara and Perttilä, 1978). Degradation of rhizobia in *npd1* nodules began around 8 DPI, just before nitrogen fixation would normally start (Sinharoy et al., 2013). Thus, the early onset of nodule senescence in *npd1* mutants presumably occurred via another mechanism (or mechanisms). Marked cellular differences between developmental and stress-induced nodule senescence in *Medicago* have been previously reported in Pérez Guerra et al. (2010). According to Pérez Guerra et al. (2010), some of the most distinct features of stress-induced senescence are condensation of the bacteroid content and symbiosome space enlargement, followed by complete bacteroid degradation, with persistence of the PBM. By contrast, in developmental senescence, symbiosomes undergo complete disintegration, with no visible PBM in transmission electron micrographs. The *npd1* phenotype most closely resembles stress-induced senescence due to its premature onset and PBM persistence after bacteroid degradation (Fig. 5; Supplemental Fig. S14).

An apparently unique feature of the *npd1* mutant is its strain-dependent symbiotic phenotype. All *npd1* mutant nodules harboring strain Sm1021 were small, round, and white, while all nodules occupied by strain Sm2011 accumulated brown material of a phenolic nature (Fig. 6, B and E; Supplemental Fig. S7, C and D). Strain SmABS7 elicited a mixture of pink and brown nodules on the *npd1* mutant, while strain Rm41 triggered the development of only large, pink, and more numerous nodules than in the wild type (Fig. 6, C–E). Most surprising was the observation that *npd1* plants harboring Rm41 rhizobia produced higher shoot biomass than the Rm41-inoculated wild type (Fig. 6F). These findings suggest that MtNPD1 can have a negative effect on nodulation and SNF, depending on the bacterial strain. Previously, it was reported that, similar to the wild type, the *dnf2* mutant grown on agarose or Phytagel plates developed nitrogen-fixing nodules (Berrabah et al., 2014a). When a plant defense elicitor was added to these growth substrates, Fix nodules developed, demonstrating that variations in growth conditions can dramatically modulate nodule development and nitrogen fixation. The distinct, strain-dependent phenotypes of *npd1* mutants suggest that MtNPD1 may be a modulator of plant immunity during nodulation and

an important determinant of symbiotic specificity. Bacterial NFs, surface exopolysaccharides, and secreted proteins all have been shown to control specificity in legume-rhizobia symbioses (Lerouge et al., 1990; Jones et al., 2007), but less is known about host specificity determinants. In Lotus, the LysM domains of NF receptor proteins (NFR1 and NFR5) have been shown to mediate the symbiotic host range (Radutoiu et al., 2007). The soybean *Rj2* gene encoding a Toll/interleukin-1 receptor/nucleotide-binding site/Leu-rich repeat class of proteins has been shown to restrict nodulation by a group of *Bradyrhizobium japonicum* strains (Yang et al., 2010). The *Nitrogen fixation specificity 2* gene encoding an NCR peptide was recently shown to act as a negative regulator of symbiotic persistence in a strain-specific manner in *M. truncatula* (Wang et al., 2017). In wild-type *Medicago*, when *MtNPD1* is expressed at normal levels, the host permits entry and accommodates various rhizobial strains, possibly due to a role of MtNPD1 in suppressing host defense. Nonetheless, different rhizobial strains nodulate wild-type R108 with various degrees of efficiency, as shown by the differences in nodule numbers and nodule categories among the three tested strains (Fig. 6, E and F). Without MtNPD1, *npd1* mutants appear to be more selective of symbiotic partners, mounting defense responses against some strains (e.g. Sm2011 and Sm1021), while favoring others (Rm41 and SmABS7). Future work on the functional characterization of *MtNPD1* will enable a better understanding of its putative role in host-strain specificity.

MtNPD1 expression was induced very early during the infection process (Fig. 8; Supplemental Figs. S8 and S10). *MtNPD1* was expressed in infected root hair cells and accompanied bacterial infection within nodule primordia. The in situ expression pattern of a promoter-GUS fusion is in agreement with the early onset of *MtNPD1* expression, as shown by a time course of nodule development and in dissected nodule zones (Fig. 8, A and B). In nitrogen-fixing nodules (10 DPI), *MtNPD1* is expressed in both the infection zone and the nitrogen-fixation zone, in agreement with transcriptomic data generated from laser-capture microdissected nodule tissue (Limpens et al., 2013; Roux et al., 2014).

MtNPD1 was not expressed in mutant nodules in which rhizobia were not released from ITs, such as those of the *TE7* (*ipd3*) mutant, or in wild-type nodules infected by *exoA* mutant rhizobia (Fig. 9). On the other hand, *MtNPD1* was expressed in nodules in which rhizobia were released but did not differentiate fully, as in the *dnf1* to *dnf7* mutants, and also in wild-type nodules infected by *bacA* (defective in terminal differentiation) and *fixJ* mutant rhizobia (which differentiate into nitrogen-fixing bacteroids but undergo early senescence). The expression pattern of *MtNPD1* in various mutant nodules recapitulates, to a large extent, that of *RSD*, which is also indispensable for bacteroid differentiation and nitrogen fixation, and for delaying the onset of stress-induced senescence (Sinharoy et al., 2013). Taking into account the nodule phenotypes and expression pattern of *MtNPD1* in wild-type and various symbiotic mutants of *Medicago*, and the expression profile of various plant and bacterial genes in the *npd1* nodules, we conclude that *MtNPD1* acts downstream of rhizobial release from infection threads, and is critical for accommodation and maintenance of rhizobia in host cells.

MtNPD1 encodes a small protein of 169 amino acid residues, including a signal peptide and a PLAT domain, and is required for effective root nodule symbiosis. The *Medicago* genome contains a total of 13 single PLAT domain genes, five of which are nodule specific (the *MtNPD* gene family) and likely evolved by tandem duplication, given their close proximity on chromosome 2 (Supplemental Fig. S9) and their phylogenetic relatedness (Fig. 7). Intriguingly, loss of *MtNPD1* function was not compensated for by the other nodule-specific *MtNPD* genes, indicating that they play distinct roles in symbiosis. Putative nonredundant roles of the five *MtNPD* genes were also suggested by Trujillo et al. (2019), who identified the single PLAT domain *MtNPD* genes using a different approach: mining for lineage-specific expansions of nodule-enhanced secreted proteins. Multiplex CRISPR/Cas9 genome editing was used to generate *M. truncatula NPD* knockout lines targeting single or multiple *MtNPD* genes. Although a single gene mutant of *MtNPD1* was not described, symbiotic phenotypes of triple, quadruple, and quintuple mutant lines in which *MtNPD1* was also targeted suggested a central role played by *MtNPD1* in nodule development and prevention of early senescence.

In functional nodules, an MtNPD1:GFP fusion protein transcribed from the *MtNPD1* promoter, localized in the proximity of symbiosomes (Fig. 10, D–F). When ectopically expressed under the 35S promoter in tobacco epidermal cells, MtNPD1 colocalized with the endoplasmic reticulum, and also with vacuoles, suggesting that vacuole-like compartments may be the final destination of MtNPD1 (Supplemental Fig. S13 A). No colocalization was observed with Golgi stacks, suggesting that MtNPD1 might belong to a Golgi-independent secretory pathway (Supplemental Fig. S13 C).

The observed GFP signal in symbiosomes does not rule out the possibility that MtNPD1 may localize to the endoplasmic reticulum and be subsequently redirected to symbiosomes. The fact that it has a signal peptide makes it plausible that MtNPD1 is processed in the endoplasmic reticulum before reaching the symbiosomes. It is noteworthy that NAD1 and MtNDR1 do localize to the endoplasmic reticulum, suggesting that endoplasmic reticulum-localized proteins may play a key role in suppressing defense responses in developing nodules (Wang et al., 2016).

In summary, MtNPD1 is critical for the accommodation of, and nitrogen fixation by, specific strains of rhizobia in *Medicago* nodules. MtNPD1 appears to be an important determinant of host-strain specificity and its discovery opens a new line of research into this important aspect of nitrogen-fixing symbiosis.

MATERIALS AND METHODS

Plant Growth and Symbiotic Screening Conditions

Seed germination and growth conditions were carried out as previously described (Pislariu et al., 2012), with seedlings being sown in Ray Leach Conetainers (Stuewue & Sons) containing a 2:1 ratio of turface to vermiculite. Nodulation experiments were carried out using the following strains: *Sinorhizobium meliloti* ABS7, Sm1021 (Meade et al., 1982), Sm2011 (Rosenberg et al., 1981), SmRm41 (Kondorosi et al., 1977), Sm1021 carrying the pXLGD4 plasmid (Leong et al., 1985; Boivin et al., 1990), Sm1021 carrying the mCherry reporter plasmid, and Sm1022 expressing *nifH*:*GFP*. Rhizobial inocula were prepared as described (Pislariu et al., 2012). The following rhizobial mutants were also used in this study: *exoA* (Leigh et al., 1985) and *bacA* (Ferguson et al., 2002).

Identification of *MtNPD1* and Aadditional *Tnt1*-Insertion Alleles

All *npd1* alleles were isolated from the tobacco (*Nicotiana tabacum*) retrotransposon *Tnt1*-insertion mutant population of *Medicago truncatula* (Tadege et al., 2008). One of the *fix*$^-$ symbiotic mutants described previously (Pislariu et al., 2012) was identified in line NF4608. Retrieval of *Tnt1* FSTs was carried out as described (Liu and Whittier, 1995; Cheng et al., 2011). Additional *Tnt1*-insertion alleles were identified in NF6576 and NF9985 by PCR reverse screening of the *Medicago Tnt1*-insertion mutant population. Primers used in screening are listed in Supplemental Table S2. All *npd1* mutant alleles were backcrossed to wild-type R108 twice to generate heterozygous F1 and segregating F2 progeny, as described (Taylor et al., 2011). The *MtNPD1* genomic sequence was amplified using theNPD1-ORF-F1 ENTR and NPD1-ORF-R3 primers, cloned into the pENTR-D-TOPO vector, and subsequently sequenced. ORF in the primer names indicates that the same primers were used to aplify the MtNPD1 open reading frame.

Characterization of the Symbiotic Phenotype of *npd1* Mutants, Histochemistry, and Microscopy

The symbiotic phenotype in *npd1* mutants was first assessed visually, and whole plants were photographed using a DXM1200C digital camera (Nikon Instruments). Nodulated roots were also imaged using an Olympus SZX12 stereomicroscope (Olympus) equipped with a DXM1200C digital camera (Nikon Instruments). Rhizobia carrying the *hemA:lacZ* reporter were stained with 5-bromo-4-chloro-3-indolyl-b-D-galactopyranoside (Boivin et al., 1990) and further processed as described in Pislariu et al. (2012). Nodules harvested at 10 DPI were fixed and sliced into semithin and ultrafine sections for compound and electron microscopy, as described (Sinharoy et al., 2013). Potassium permanganate ($KMnO_4$) staining was done according to Vasse et al. (1993). Digital photomicrographs were processed using Adobe Photoshop Elements 14. The symbiotic phenotype of *npd1* mutants was also assessed by confocal microscopy using a Leica TCS SP2 AOBS laser-scanning microscope. Nodule sections were stained with the fluorescent DNA dye Syto13 (Life Technologies; Haynes et al., 2004), rinsed with PIPES, and subsequently stained with 0.01% (w/v) Calcofluor-white (Life Technologies) to visualize rhizobia and plant cell walls. Staining with FM 1-43 was carried out following the manufacturer's instructions (Life Technologies). For live/dead staining of rhizobia, freshly sliced sections were stained with a mixture of 5 μM Syto9 and 30 μM PI, as previously described (Haag et al., 2011).

Complementation of the *npd1* Mutant Phenotype

The *MtNPD1* open reading frame was amplified from nodule complementary DNA and cloned into the Gateway pB7WG2D.1 binary vector (Invitrogen), which constitutively expresses GFP as a selection marker of transgenic roots (Karimi et al., 2002). An empty vector was used as a control for hairy root transformation. The *Rhizobium rhizogenes* strain Arqua1 was transformed with the obtained vectors, and used to generate composite *Medicago* plants according to Boisson-Dernier et al. (2001) and Sinharoy et al. (2015). Screening for transgenic (green fluorescent), nodulated roots was done using an Olympus SZX12 fluorescence stereomicroscope. To evaluate the integrity of rhizobia, nodule sections were observed by confocal microscopy.

Analysis of Nitrogen Fixation by Microscopy and the Acetylene Reduction Assay

Wild-type and *npd1-1* mutant plants were inoculated with an *S. meliloti* strain expressing GFP under the control of the nitrogenase reductase (*nifH*) promoter (*nifH:GFP*). At 21 DPI, nodules were sectioned and observed using an Olympus BX41 compound fluorescent microscope. Photomicrographs were acquired using an Olympus DP72 camera.

The acetylene reduction assay was carried out as previously described (Oke and Long, 1999). Briefly, after growing under symbiotic conditions, entire root systems were transferred onto sterile Whatman paper strips placed inside 12-mL glass vials containing 2 mL of Broughton & Dilworth nutrient solution (Broughton and Dilworth, 1971). The tubes were sealed with Suba-Seal septum stoppers (Chemglass Life Sciences). Samples were incubated in the presence of 10% (v/v) acetylene at 28°C for 15–20 h. Ethylene and acetylene concentrations were measured using an Agilent 7890A gas chromatograph (Agilent Technologies).

MtNPD1 promoter activity

A 1,320 bp region upstream of the ATG start codon was amplified from R108 genomic DNA and cloned into the Gateway binary destination vector pBGWFS7.0 (Karimi et al., 2002) to generate a p*MtNPD1*:GUS fusion. The plasmid was deployed into *M. truncatula* via *R. rhizogenes* (Arqua1) transformation (Boisson-Dernier et al., 2001). Composite plants were inoculated with *S. meliloti* Sm2011/*pXLDG4* containing the constitutive *hemA:lacZ* gene. Histochemical staining with X-Gluc (5-bromo-4-chloro-3-indoxyl-β-D-glucuronide cyclohexylammonium salt; Gold Biotechnology) and with Magenta-Gal (5-bromo-6-chloro-3-indoxyl β-D- galactopyranoside; Gold Biotechnology) were carried out as described (Pislariu and Dickstein, 2007).

Localization of MtNPD1 in Root Nodules

A genomic segment containing the *MtNPD1* promoter, exons, and introns, was amplified from genomic DNA using the NPD1p-F and cGFP-NPD1-R1 primers (Supplemental Table S2). The PCR product was cloned into the Gateway pRRcGFP destination vector (Kryvoruchko et al., 2016). A control construct for the localization of free GFP (*pMtNPD1p:GFP*) was also generated. The obtained vectors were transferred to *Medicago* via *R. rhizogenes* transformation. Composite plants were inoculated with *S. meliloti* Sm1021-mCherry. Hand-sliced transgenic nodule samples were observed with a laser scanning confocal microscope (Leica SP2 TCS AOBS; Leica Microsystems). Composite plants were also evaluated for complementation by pMtNPD1:MtNPD1:GFP, as described above, by assessing plant appearance and acetylene reduction activity.

Transient Expression in Tobacco

Rhizobium tumefaciens C58C1 carrying p35S:MtNDP1:RFP or the empty vector pB7RWG2.0 (Karimi et al., 2002) was vacuum infiltrated into tobacco leaves as previously described (Goodin et al., 2002). The following constructs were used for coinfiltration and colocalization experiments: p35S:sGFP (secreted GFP; Chiu et al., 1996); p35S:ST:sGFP (Boevink et al., 1998); p35S:mGFP5-ER (Haseloff et al., 1997); and p35S:γ-TIP:CFP (Nelson et al., 2007). Confocal images were acquired using a Leica SP2 TCS AOBS laser scanning confocal microscope (Leica Microsystems) using appropriate lasers and transmitted light and a sequential ("between lines") scanning mode.

RNA Extraction and RT-qPCR Analysis

Total RNA was extracted using the TRIZOL reagent from nodulated root systems harvested at 2, 4, 6, 8, 10, 15, and 21 DPI. Samples at 2 and 4 DPI represented root segments from the nodulation-susceptible zone. This region consisted of the root hair zone II (root hairs that had nearly finished growing), between (but not including) the growing root tip, and the zone of fully elongated root hairs, as previously defined (Gage, 2004). Only bumps and nodules were dissected out at all other time points (6–21 DPI). Tissue from at least 40 plants was harvested at each time point, and data were acquired from three independent biological replicates. To gain spatial resolution of *MtNPD1* expression during nodule development, RNA was extracted from five developmentally distinct zones: the meristem, the infection zone, the distal nitrogen fixation zone, the nitrogen fixation zone, and the senescence zone. RNA was

extracted and processed in a similar fashion from 15 DPI nodules harvested from symbiotic mutants (*dnf1*, *dnf2*, *dnf3*, *dnf4*, *dnf5*, *dnf6*, *dnf7*, and TE7 [ipd3]; Benaben et al., 1995; Mitra and Long, 2004; Starker et al., 2006), and from R108 plants inoculated with Sm1021, *exoA*, *bacA*, and *fixJ*. Gene expression was quantified by RT-qPCR as previously described (Kakar et al., 2008). Transcript levels were normalized using the mean average of three housekeeping genes: *Ubiquitin-Conjugating Enzyme-E2, MtUBC9* (*Medtr7g116940*); *Ser/Thr Phosphatase 2A regulatory subunit A, MtPDF2* (*Medtr6g084690*); and *Ubiquitin-Conjugating Enzyme, MtUBC* (*Medtr3g110110*), whose expression is stable across all samples.

Bioinformatics and Phylogenetic Analysis

The *MtNPD1* sequence in *Medicago* R108 ecotype was revealed by cloning and sequencing. The result was cross-referenced with the *M. truncatula* R108 v0.95 Assembly and with the Mt4.0 v1 A17 genome (JCVI, http://blast.jcvi.org/Medicago-Blast/index.cgi). BLAST searches of the *Medicago* genome and the NCBI database using the MtNPD1 deduced amino acid sequence were carried out to identify single PLAT domain plant proteins with similar organization (Altschul et al., 1990). A representative sample of 40 proteins including MtNPD1, were aligned with ClustalW, and an unrooted maximum-likelihood phylogenetic tree was generated using the PhyML tool and the LG substitution model (Le and Gascuel, 2008) in the Geneious 10.2.5 software (Biomatters Ltd.).

Statistical Analysis

Student's *t* test was used to compare statistical significance between observed differences. The analysis was carried out using the Microsoft Excel T.TEST function, considering two-tailed distribution and unequal variances. One-way ANOVA tests were also carried out for multiple comparisons. P values ≤ 0.05 were considered statistically significant. Bar graphs and statistical analyses were carried out using Prism 7 (GraphPad).

Accession Numbers

The *MtNPD1* gene sequence was submitted to GenBank and assigned accession number KX579942. Accession numbers of other major genes discussed in the paper are listed in Supplemental Table S5.

SUPPLEMENTAL MATERIAL

The following supplemental information is available:

Supplemental Figure S1. Nodule development and early infection in the mutant isolated from NF4608.

Supplemental Figure S2. Alignment between the *MtNPD1*_R108 CDS and *MtNPD1*_A17.

Supplemental Figure S3. Alignment between the *MtNPD1*_R108 CDS and the R108 v0.95 genome assembly (http://medicago.jcvi.org).

Supplemental Figure S4. Nitrate complements the *npd1* symbiotic phenotype.

Supplemental Figure S5. Confocal imaging of Syto13-stained rhizobia.

Supplemental Figure S6. Rhizobia undergo quick degradation in *npd1* nodules.

Supplemental Figure S7. *npd1-1* nodules inoculated with Sm2011 accumulate brown material of a polyphenolic nature.

Supplemental Figure S8. *MtNPD1*, *MtNPD2*, *MtNPD3*, *MtNPD4*, and *MtNPD5* genes are expressed exclusively in root nodules.

Supplemental Figure S9. *MtNPD1* belongs to a cluster of PLAT-encoding nodule-specific genes.

Supplemental Figure S10. Expression pattern of the *MtNPD1* promoter-*GUS* fusion in unfixed *M. truncatula* nodules.

Supplemental Figure S11. Relative expression of bacterial genes in *npd1-1*.

Supplemental Figure S12. A *pMtNPD1:MtNPD1:GFP* construct complements the symbiotic phenotype of the *npd1-1* mutant.

Supplemental Figure S13. MtNPD1:RFP fusion driven by the 35S promoter localizes to vacuoles and the endoplasmic reticulum in tobacco epidermal cells.

Supplemental Figure S14. Symbiosome degradation in *npd1* nodules.

Supplemental Figure S15. Relative expression of defense-related symbiotic genes.

Supplemental Table S1. FSTs retrieved from NF4608, NF6576, and NF9985.

Supplemental Table S2. Primers used in this work.

Supplemental Table S3. PLAT domain proteins in the *Medicago* genome.

Supplemental Table S4. PLAT domain proteins in plants.

Supplemental Table S5. Accession numbers of major genes mentioned in the article.

ACKNOWLEDGMENTS

We thank Pascal Ratet, Kirankumar Mysore, and Million Tadege for developing the Medicago tobacco retrotransposon (*Tnt1*)-insertion mutant population. We thank Jiangqi Wen and Xiaofei Cheng for screening the *Tnt1*-insertion population for additional *npd1* alleles, Mark Taylor for performing genetic crosses, the greenhouse personnel (Janie Gallaway, Colleen Elles, Frank Coker, and Vicki Barrett) for maintaining the *Tnt1*-insertion lines, Shulan Zhang for thermal asymmetric interlaced PCR, assistance with nodulation assays, and DNA extractions, Jiangqi Wen for analysis of FST data in line NF4608, and Yixuan (Jack) Wen for technical assistance. We also thank Yuhong Tang and the Noble Foundation Genomics Core Facility for sequencing. We thank Kathryn Jones for providing *S. meliloti* Sm1021 and *exoA* strains, Sharon Long and Melanie Barnett for providing the *bacA* and *fixJ* strains, Phil Poole for providing mCherry-labeled rhizobia, and Pascal Ratet for providing the Rm41 strain.

Received January 7, 2019; accepted April 22, 2019; published May 6, 2019.

LITERATURE CITED

Altschul SF, Gish W, Miller W, Myers EW, Lipman DJ (1990) Basic local alignment search tool. J Mol Biol **215:** 403–410

Ardourel M, Demont N, Debellé F, Maillet F, de Billy F, Promé JC, Dénarié J, Truchet G (1994) *Rhizobium meliloti* lipooligosaccharide nodulation factors: Different structural requirements for bacterial entry into target root hair cells and induction of plant symbiotic developmental responses. Plant Cell **6:** 1357–1374

Benaben V, Duc G, Lefebvre V, Huguet T (1995) *TE7*, an inefficient symbiotic mutant of *Medicago truncatula* Gaertn. cv Jemalong. Plant Physiol **107:** 53–62

Benedito VA, Torres-Jerez I, Murray JD, Andriankaja A, Allen S, Kakar K, Wandrey M, Verdier J, Zuber H, Ott T, et al (2008) A gene expression atlas of the model legume *Medicago truncatula*. Plant J **55:** 504–513

Berrabah F, Bourcy M, Cayrel A, Eschstruth A, Mondy S, Ratet P, Gourion B (2014a) Growth conditions determine the DNF2 requirement for symbiosis. PLoS One **9:** e91866

Berrabah F, Bourcy M, Eschstruth A, Cayrel A, Guefrachi I, Mergaert P, Wen J, Jean V, Mysore KS, Gourion B, Ratet P (2014b) A nonRD receptor-like kinase prevents nodule early senescence and defense-like reactions during symbiosis. New Phytol **203:** 1305–1314

Berrabah F, Ratet P, Gourion B (2015) Multiple steps control immunity during the intracellular accommodation of rhizobia. J Exp Bot **66:** 1977–1985

Beynon JL, Williams MK, Cannon FC (1988) Expression and functional analysis of the *Rhizobium meliloti nifA* gene. EMBO J **7:** 7–14

Boevink P, Oparka K, Santa Cruz S, Martin B, Betteridge A, Hawes C (1998) Stacks on tracks: The plant Golgi apparatus traffics on an actin/ER network. Plant J **15:** 441–447

Boisson-Dernier A, Chabaud M, Garcia F, Bécard G, Rosenberg C, Barker DG (2001) *Agrobacterium rhizogenes*-transformed roots of *Medicago truncatula* for the study of nitrogen-fixing and endomycorrhizal symbiotic associations. Mol Plant Microbe Interact **14:** 695–700

Boivin C, Camut S, Malpica CA, Truchet G, Rosenberg C (1990) *Rhizobium meliloti* genes encoding catabolism of trigonelline are induced under symbiotic conditions. Plant Cell **2:** 1157–1170

Bourcy M, Brocard L, Pislariu CI, Cosson V, Mergaert P, Tadege M, Mysore KS, Udvardi MK, Gourion B, Ratet P (2013) *Medicago truncatula* DNF2 is a PI-PLC-XD-containing protein required for bacteroid persistence and prevention of nodule early senescence and defense-like reactions. New Phytol **197:** 1250–1261

Brewin N (2004) Plant cell wall remodeling in the rhizobium-legume symbiosis. Crit Rev Plant Sci **23:** 293–316

Broughton WJ, Dilworth MJ (1971) Control of leghaemoglobin synthesis in snake beans. Biochem J **125:** 1075–1080

Cao Y, Halane MK, Gassmann W, Stacey G (2017) The role of plant innate immunity in the legume-rhizobium symbiosis. Annu Rev Plant Biol **68:** 535–561

Cheng X, Wen J, Tadege M, Ratet P, Mysore KS (2011) Reverse genetics in *Medicago truncatula* using *Tnt1* insertion mutants. Methods Mol Biol **678:** 179–190

Chiu W, Niwa Y, Zeng W, Hirano T, Kobayashi H, Sheen J (1996) Engineered GFP as a vital reporter in plants. Curr Biol **6:** 325–330

Couzigou JM, Zhukov V, Mondy S, Abu el Heba G, Cosson V, Ellis TH, Ambrose M, Wen J, Tadege M, Tikhonovich I, et al (2012) *NODULE ROOT* and *COCHLEATA* maintain nodule development and are legume orthologs of Arabidopsis *BLADE-ON-PETIOLE* genes. Plant Cell **24:** 4498–4510

David M, Daveran ML, Batut J, Dedieu A, Domergue O, Ghai J, Hertig C, Boistard P, Kahn D (1988) Cascade regulation of *nif* gene expression in *Rhizobium meliloti.* Cell **54:** 671–683

Ferguson GP, Roop II RM, Walker GC (2002) Deficiency of a *Sinorhizobium meliloti BacA* mutant in alfalfa symbiosis correlates with alteration of the cell envelope. J Bacteriol **184:** 5625–5632

Fukai E, Soyano T, Umehara Y, Nakayama S, Hirakawa H, Tabata S, Sato S, Hayashi M (2012) Establishment of a *Lotus japonicus* gene tagging population using the exon-targeting endogenous retrotransposon *LORE1.* Plant J **69:** 720–730

Gage DJ (2004) Infection and invasion of roots by symbiotic, nitrogen-fixing rhizobia during nodulation of temperate legumes. Microbiol Mol Biol Rev **68:** 280–300

Geurts R, Bisseling T (2002) Rhizobium nod factor perception and signalling. Plant Cell **14**(Suppl): S239–S249

Glazebrook J, Ichige A, Walker GC (1993) A *Rhizobium meliloti* homolog of the *Escherichia coli* peptide-antibiotic transport protein SbmA is essential for bacteroid development. Genes Dev **7:** 1485–1497

Goodin MM, Dietzgen RG, Schichnes D, Ruzin S, Jackson AO (2002) pGD vectors: Versatile tools for the expression of green and red fluorescent protein fusions in agroinfiltrated plant leaves. Plant J **31:** 375–383

Graham PH, Vance CP (2003) Legumes: Importance and constraints to greater use. Plant Physiol **131:** 872–877

Haag AF, Baloban M, Sani M, Kerscher B, Pierre O, Farkas A, Longhi R, Boncompagni E, Hérouart D, Dall'angelo S, et al (2011) Protection of *Sinorhizobium* against host cysteine-rich antimicrobial peptides is critical for symbiosis. PLoS Biol **9:** e1001169

Haseloff J, Siemering KR, Prasher DC, Hodge S (1997) Removal of a cryptic intron and subcellular localization of green fluorescent protein are required to mark transgenic *Arabidopsis* plants brightly. Proc Natl Acad Sci USA **94:** 2122–2127

Haynes JG, Czymmek KJ, Carlson CA, Veereshlingam H, Dickstein R, Sherrier DJ (2004) Rapid analysis of legume root nodule development using confocal microscopy. New Phytol **163:** 661–668

He J, Benedito VA, Wang M, Murray JD, Zhao PX, Tang Y, Udvardi MK (2009) The *Medicago truncatula* gene expression atlas web server. BMC Bioinformatics **10:** 441

Hirsch AM, Bang M, Ausubel FM (1983) Ultrastructural analysis of ineffective alfalfa nodules formed by *nif:Tn5* mutants of *Rhizobium meliloti.* J Bacteriol **155:** 367–380

Horváth B, Yeun LH, Domonkos A, Halász G, Gobbato E, Ayaydin F, Miró K, Hirsch S, Sun J, Tadege M, et al (2011) *Medicago truncatula IPD3* is a member of the common symbiotic signaling pathway required for rhizobial and mycorrhizal symbioses. Mol Plant Microbe Interact **24:** 1345–1358

Horváth B, Domonkos Á, Kereszt A, Szűcs A, Ábrahám E, Ayaydin F, Bóka K, Chen Y, Chen R, Murray JD, Udvardi et al (2015) Loss of the nodule-specific cysteine rich peptide, NCR169, abolishes symbiotic nitrogen fixation in the *Medicago truncatula dnf7* mutant. Proc Natl Acad Sci USA **112:** 15232–15237

Hyun TK, van der Graaff E, Albacete A, Eom SH, Großkinsky DK, Böhm H, Janschek U, Rim Y, Ali WW, Kim SY, et al (2014) The *Arabidopsis* PLAT domain protein1 is critically involved in abiotic stress tolerance. PLoS One **9:** e112946

Jones KM, Kobayashi H, Davies BW, Taga ME, Walker GC (2007) How rhizobial symbionts invade plants: The *Sinorhizobium-Medicago* model. Nat Rev Microbiol **5:** 619–633

Jones KM, Sharopova N, Lohar DP, Zhang JQ, VandenBosch KA, Walker GC (2008) Differential response of the plant *Medicago truncatula* to its symbiont *Sinorhizobium meliloti* or an exopolysaccharide-deficient mutant. Proc Natl Acad Sci USA **105:** 704–709

Kakar K, Wandrey M, Czechowski T, Gaertner T, Scheible WR, Stitt M, Torres-Jerez I, Xiao Y, Redman JC, Wu HC, et al (2008) A community resource for high-throughput quantitative RT-PCR analysis of transcription factor gene expression in *Medicago truncatula.* Plant Methods **4:** 18

Kalandadze AG, Bushara SA, Vassetzky YS, Jr., Razin SV (1990) Characterization of DNA pattern in the site of permanent attachment to the nuclear matrix located in the vicinity of replication origin. Biochem Biophys Res Commun **168:** 9–15

Karimi M, Inzé D, Depicker A (2002) GATEWAY vectors for *Agrobacterium*-mediated plant transformation. Trends Plant Sci **7:** 193–195

Kim M, Chen Y, Xi J, Waters C, Chen R, Wang D (2015) An antimicrobial peptide essential for bacterial survival in the nitrogen-fixing symbiosis. Proc Natl Acad Sci USA **112:** 15238–15243

Kondorosi A, Kiss GB, Forrai T, Vincze E, Banfalvi Z (1977) Circular linkage map of *Rhizobium meliloti* chromosome. Nature **268:** 525–527

Kryvoruchko IS, Sinharoy S, Torres-Jerez I, Sosso D, Pislariu CI, Guan D, Murray J, Benedito VA, Frommer WB, Udvardi MK (2016) MtSWEET11, a nodule-specific sucrose transporter of *Medicago truncatula.* Plant Physiol **171:** 554–565

Le SQ, Gascuel O (2008) An improved general amino acid replacement matrix. Mol Biol Evol **25:** 1307–1320

Lee SC, Kim SH, An SH, Yi SY, Hwang BK (2006) Identification and functional expression of the pepper pathogen-induced gene, *CAPIP2,* involved in disease resistance and drought and salt stress tolerance. Plant Mol Biol **62:** 151–164

Lehtovaara P, Perttilä U (1978) Bile-pigment formation from different leghaemoglobins. Methine-bridge specificity of coupled oxidation. Biochem J **176:** 359–364

Leigh JA, Signer ER, Walker GC (1985) Exopolysaccharide-deficient mutants of *Rhizobium meliloti* that form ineffective nodules. Proc Natl Acad Sci USA **82:** 6231–6235

Leong SA, Williams PH, Ditta GS (1985) Analysis of the 5′ regulatory region of the gene for δ-aminolevulinic acid synthetase of *Rhizobium meliloti.* Nucleic Acids Res **13:** 5965–5976

Lerouge P, Roche P, Faucher C, Maillet F, Truchet G, Promé JC, Dénarié J (1990) Symbiotic host-specificity of *Rhizobium meliloti* is determined by a sulphated and acylated glucosamine oligosaccharide signal. Nature **344:** 781–784

Limpens E, Franken C, Smit P, Willemse J, Bisseling T, Geurts R (2003) LysM domain receptor kinases regulating rhizobial Nod factor-induced infection. Science **302:** 630–633

Limpens E, Moling S, Hooiveld G, Pereira PA, Bisseling T, Becker JD, Küster H (2013) Cell- and tissue-specific transcriptome analyses of *Medicago truncatula* root nodules. PLoS One **8:** e64377

Liu YG, Whittier RF (1995) Thermal asymmetric interlaced PCR: Automatable amplification and sequencing of insert end fragments from P1 and YAC clones for chromosome walking. Genomics **25:** 674–681

Marchler-Bauer A, Derbyshire MK, Gonzales NR, Lu S, Chitsaz F, Geer LY, Geer RC, He J, Gwadz M, Hurwitz DI, et al (2015) CDD: NCBI's conserved domain database. Nucleic Acids Res **43:** D222–D226

Meade HM, Long SR, Ruvkun GB, Brown SE, Ausubel FM (1982) Physical and genetic characterization of symbiotic and auxotrophic mutants of *Rhizobium meliloti* induced by transposon *Tn5* mutagenesis. J Bacteriol **149:** 114–122

Mergaert P, Nikovics K, Kelemen Z, Maunoury N, Vaubert D, Kondorosi A, Kondorosi E (2003) A novel family in *Medicago truncatula* consisting of more than 300 nodule-specific genes coding for small, secreted polypeptides with conserved cysteine motifs. Plant Physiol **132:** 161–173

Mergaert P, Uchiumi T, Alunni B, Evanno G, Cheron A, Catrice O, Mausset AE, Barloy-Hubler F, Galibert F, Kondorosi A, et al(2006)

Eukaryotic control on bacterial cell cycle and differentiation in the *Rhizobium*-legume symbiosis. Proc Natl Acad Sci USA **103:** 5230–5235

Mitra RM, Long SR (2004) Plant and bacterial symbiotic mutants define three transcriptionally distinct stages in the development of the *Medicago truncatula/Sinorhizobium meliloti* symbiosis. Plant Physiol **134:** 595–604

Nelson BK, Cai X, Nebenführ A (2007) A multicolored set of in vivo organelle markers for co-localization studies in *Arabidopsis* and other plants. Plant J **51:** 1126–1136

Oke V, Long SR (1999) Bacterial genes induced within the nodule during the *Rhizobium*-legume symbiosis. Mol Microbiol **32:** 837–849

Oldroyd GED, Murray JD, Poole PS, Downie JA (2011) The rules of engagement in the legume-rhizobial symbiosis. Annu Rev Genet **45:** 119–144

Pérez Guerra JC, Coussens G, De Keyser A, De Rycke R, De Bodt S, Van De Velde W, Goormachtig S, Holsters M (2010) Comparison of developmental and stress-induced nodule senescence in *Medicago truncatula.* Plant Physiol **152:** 1574–1584

Pislariu CI, Dickstein R (2007) An IRE-like AGC kinase gene, *MtIRE*, has unique expression in the invasion zone of developing root nodules in *Medicago truncatula.* Plant Physiol **144:** 682–694

Pislariu CI, Murray JD, Wen J, Cosson V, Muni RR, Wang M, Benedito VA, Andriankaja A, Cheng X, Jerez IT, et al (2012) A *Medicago truncatula* tobacco retrotransposon insertion mutant collection with defects in nodule development and symbiotic nitrogen fixation. Plant Physiol **159:** 1686–1699

Radutoiu S, Madsen LH, Madsen EB, Jurkiewicz A, Fukai E, Quistgaard EMH, Albrektsen AS, James EK, Thirup S, Stougaard J (2007) LysM domains mediate lipochitin-oligosaccharide recognition and *Nfr* genes extend the symbiotic host range. EMBO J **26:** 3923–3935

Rey T, Nars A, Bonhomme M, Bottin A, Huguet S, Balzergue S, Jardinaud MF, Bono JJ, Cullimore J, Dumas B, et al (2013) NFP, a LysM protein controlling Nod factor perception, also intervenes in *Medicago truncatula* resistance to pathogens. New Phytol **198:** 875–886

Rosenberg C, Boistard P, Dénarié J, Casse-Delbart F (1981) Genes controlling early and late functions in symbiosis are located on a megaplasmid in *Rhizobium meliloti.* Mol Gen Genet **184:** 326–333

Roux B, Rodde N, Jardinaud MF, Timmers T, Sauviac L, Cottret L, Carrère S, Sallet E, Courcelle E, Moreau S, et al (2014) An integrated analysis of plant and bacterial gene expression in symbiotic root nodules using laser-capture microdissection coupled to RNA sequencing. Plant J **77:** 817–837

Ruvkun GB, Sundaresan V, Ausubel FM (1982) Directed transposon *Tn5* mutagenesis and complementation analysis of *Rhizobium meliloti* symbiotic nitrogen fixation genes. Cell **29:** 551–559

Sato S, Nakamura Y, Kaneko T, Asamizu E, Kato T, Nakao M, Sasamoto S, Watanabe A, Ono A, Kawashima K, et al (2008) Genome structure of the legume, *Lotus japonicus.* DNA Res **15:** 227–239

Shin R, An JM, Park CJ, Kim YJ, Joo S, Kim WT, Paek KH (2004) *Capsicum annuum* tobacco mosaic virus-induced clone 1 expression perturbation alters the plant's response to ethylene and interferes with the redox homeostasis. Plant Physiol **135:** 561–573

Sinharoy S, Torres-Jerez I, Bandyopadhyay K, Kereszt A, Pislariu CI, Nakashima J, Benedito VA, Kondorosi E, Udvardi MK (2013) The C2H2 transcription factor regulator of symbiosome differentiation represses transcription of the secretory pathway gene VAMP721a and promotes symbiosome development in *Medicago truncatula.* Plant Cell **25:** 3584–3601

Sinharoy S, Pislariu CI, Udvardi MK (2015) A high-throughput RNA interference (RNAi)-based approach using hairy roots for the study of plant-rhizobia interactions. Methods Mol Biol **1287:** 159–178

Sinharoy S, Liu C, Breakspear A, Guan D, Shailes S, Nakashima J, Zhang S, Wen J, Torres-Jerez I, Oldroyd G, et al (2016) A *Medicago truncatula* cystathionine-β-synthase-like domain-containing protein is required for rhizobial infection and symbiotic nitrogen fixation. Plant Physiol **170:** 2204–2217

Starker CG, Parra-Colmenares AL, Smith L, Mitra RM, Long SR (2006) Nitrogen fixation mutants of *Medicago truncatula* fail to support plant and bacterial symbiotic gene expression. Plant Physiol **140:** 671–680

Tadege M, Wen J, He J, Tu H, Kwak Y, Eschstruth A, Cayrel A, Endre G, Zhao PX, Chabaud M, et al (2008) Large-scale insertional mutagenesis using the *Tnt1* retrotransposon in the model legume *Medicago truncatula.* Plant J **54:** 335–347

Tang H, Krishnakumar V, Bidwell S, Rosen B, Chan A, Zhou S, Gentzbittel L, Childs KL, Yandell M, Gundlach H, et al (2014) An improved genome release (version Mt4.0) for the model legume *Medicago truncatula.* BMC Genomics **15:** 312

Taylor M, Blaylock L, Nakashima J, McAbee D, Ford J, Harrison M, Udvardi M (2011) Medicago truncatula hybridization: Supplemental videos. *In* U Mathesius, EP Journet, LWA Sumner, eds, Medicago truncatula Handbook Version July 2011. Noble Research Institute, Ardmore, OK, pp 1-5, https://www.noble.org/globalassets/docs/medicago-handbook/hybridization.pdf

Trujillo DI, Silverstein KAT, Young ND (2019) Nodule-specific PLAT domain proteins are expanded in the *Medicago* lineage and required for nodulation. New Phytol **222:** 1538–1550

Udvardi MK, Day DA (1997) Metabolite transport across symbiotic membranes of legume nodules. Annu Rev Plant Physiol Plant Mol Biol **48:** 493–523

Udvardi M, Poole PS (2013) Transport and metabolism in legume-rhizobia symbioses. Annu Rev Plant Biol **64:** 781–805

Van de Velde W, Guerra JCP, De Keyser A, De Rycke R, Rombauts S, Maunoury N, Mergaert P, Kondorosi E, Holsters M, Goormachtig S (2006) Aging in legume symbiosis. A molecular view on nodule senescence in *Medicago truncatula.* Plant Physiol **141:** 711–720

Van de Velde W, Zehirov G, Szatmari A, Debreczeny M, Ishihara H, Kevei Z, Farkas A, Mikulass K, Nagy A, Tiricz H, et al (2010) Plant peptides govern terminal differentiation of bacteria in symbiosis. Science **327:** 1122–1126

Vasse J, de Billy F, Camut S, Truchet G (1990) Correlation between ultrastructural differentiation of bacteroids and nitrogen fixation in alfalfa nodules. J Bacteriol **172:** 4295–4306

Vasse J, de Billy F, Truchet G (1993) Abortion of infection during the *Rhizobium meliloti*-alfalfa symbiotic interaction is accompanied by a hypersensitive reaction. Plant J **4:** 555–566

Veereshlingam H, Haynes JG, Penmetsa RV, Cook DR, Sherrier DJ, Dickstein R (2004) *nip*, a symbiotic *Medicago truncatula* mutant that forms root nodules with aberrant infection threads and plant defense-like response. Plant Physiol **136:** 3692–3702

Wang C, Yu H, Luo L, Duan L, Cai L, He X, Wen J, Mysore KS, Li G, Xiao A, et al (2016) *NODULES WITH ACTIVATED DEFENSE 1* is required for maintenance of rhizobial endosymbiosis in *Medicago truncatula.* New Phytol **212:** 176–191

Wang D, Griffitts J, Starker C, Fedorova E, Limpens E, Ivanov S, Bisseling T, Long S (2010) A nodule-specific protein secretory pathway required for nitrogen-fixing symbiosis. Science **327:** 1126–1129

Wang Q, Yang S, Liu J, Terecskei K, Ábrahám E, Gombár A, Domonkos Á, Szűcs A, Körmöczi P, Wang T, Fodor L, Mao L, et al (2017) Host-secreted antimicrobial peptide enforces symbiotic selectivity in *Medicago truncatula.* Proc Natl Acad Sci USA **114:** 6854–6859

Yang S, Tang F, Gao M, Krishnan HB, Zhu H (2010) *R* gene-controlled host specificity in the legume-rhizobia symbiosis. Proc Natl Acad Sci USA **107:** 18735–18740

Young ND, Debellé F, Oldroyd GED, Geurts R, Cannon SB, Udvardi MK, Benedito VA, Mayer KFX, Gouzy J, Schoof H, et al (2011) The *Medicago* genome provides insight into the evolution of rhizobial symbioses. Nature **480:** 520–524